Radical Enhanced Atomic Layer Deposition of Metals and Oxides

Antti Niskanen

Laboratory of Inorganic Chemistry
Department of Chemistry
Faculty of Science
University of Helsinki
Finland

Academic Dissertation

To be presented, with the permission of the Faculty of Science of the University of Helsinki, for public criticism in Auditorium A110 of the Department of Chemistry, A. I. Virtasen Aukio 1, on November 10th 2006 at 12 o'clock noon.

HELSINKI 2006

Supervisors

Prof. Mikko Ritala
and
Prof. Markku Leskelä
Laboratory of Inorganic Chemistry
Department of Chemistry
University of Helsinki
Helsinki, Finland

Reviewers

Dr. Stephen M. Rossnagel
IBM Research Division
Thomas J Watson Research Center
Yorktown Heights, NY
USA

and

Dr. Matti Putkonen
Laboratory of Inorganic and Analytical Chemistry
Technical University of Helsinki
Finland

Opponent

Dr. Erwin Kessels
Eindhoven University of Technology
Eindhoven
Netherlands

© Antti Niskanen 2006
ISBN 952-92-0982-7 (paperback)
ISBN 952-10-3395-9 (PDF)
http://ethesis.helsinki.fi
Yliopistopaino
Helsinki 2006

ABSTRACT

Atomic Layer Deposition (ALD) is a chemical, gas-phase thin film deposition method. It is known for its ability for accurate and precise thickness control, and uniform and conformal film growth. One area where ALD has not yet excelled is film deposition at low temperatures. Also deposition of metals, besides the noble metals, has proven to be quite challenging. To alleviate these limitations, more aggressive reactants are required.

One such group of reactants are radicals, which may be formed by dissociating gases. Dissociation is most conveniently done with a plasma source. For example, dissociating molecular oxygen or hydrogen, oxygen or hydrogen radicals are generated. The use of radicals in ALD may surmount some of the above limitations: oxide film deposition at low temperatures may become feasible if oxygen radicals are used as they are highly reactive. Also, as hydrogen radicals are very effective reducing agents, they may be used to deposit metals.

In this work, a plasma source was incorporated in an existing ALD reactor for radical generation, and the reactor was used to study five different Radical Enhanced ALD processes. The modifications to the existing reactor and the different possibilities during the modification process are discussed. The studied materials include two metals, copper and silver, and three oxides, aluminium oxide, titanium dioxide and tantalum oxide. The materials were characterized and their properties were compared to other variations of the same process, utilizing the same metal precursor, to understand what kind of effect the non-metal precursor has on the film properties and growth characteristics.

Both metals were deposited successfully, and silver for the first time by ALD. The films had low resistivity and grew conformally in the ALD mode, demonstrating that the REALD of metals is true ALD. The oxide films had exceptionally high growth rates, and aluminium oxide grew at room temperature with low cycle times and resulted in good quality films. Both aluminium oxide and titanium dioxide were deposited on natural fibres without damaging the fibre. Tantalum oxide was also deposited successfully, with good electrical properties, but at slightly higher temperature than the other two oxides, due to the evaporation temperature required by the metal precursor. Overall, the ability of REALD to deposit metallic and oxide films with high quality at low temperatures was demonstrated.

PREFACE

The experimental work for this thesis was done between 2000 and 2006 in the Laboratory of Inorganic Chemistry in the University of Helsinki. During those years I had the opportunity to know and work with a large number of fine and exceptionally talented people, to whom I want to express my gratitude.

First and foremost I wish to thank my supervisors, Professors Mikko Ritala and Markku Leskelä for their invaluable contribution to this work, and also for creating the perfect opportunities for me to grow into being a researcher. Working in your laboratory has been a privilege.

I am grateful to my co-workers and co-authors in the ALD-group, Dr. Antti Rahtu with whom I started the experiments and who also wrote the wonderful plasma reactor pulsing software, Mr. Timo Hatanpää for precursor synthesis, Dr. Kai Arstila, Dr. Timo Sajavaara and Dr. Ulrich Kreissig for doing the TOF-ERD analyses. I also want to thank the ALD-group as a whole for making everyday life in the lab so much fun.

I wish to thank my roommate Mr. Mikko Heikkilä, Mr. Markus Lautala and Mr. Tero Pilvi for their genuine friendship, good conversations, bad jokes and the inappropriate internet links. Without you life would have been very dull, both in and out of the office. Also, going to the gym with you guys is always a blast.

Sports and music are really close to my heart. I would like to express a big thank-you to the following people who have kept me in touch with these aspects of life: Markus and Hessu for the nicest times at climbing, Teppo for the go-kart races, and everyone who played floorball on Friday afternoons. I wish to offer warm thanks to Antti Karisalmi for introducing me into the band rehearsal space, Kelly Ketonen for letting me use and practice on his drum set, and Elina, Milli and Teppo for playing with me. The possibility to play music has always been fun and a lifeline at times.

Also warm thanks go to my friends and family: Teppo, Miso and Riku, my parents Lea and Martti, my sister Minna and her children Ella, Sanni and Veikko, Antti and Katja; you are all very special to me. Finally, my most loving thanks go to Kaisa: you've been there for me whenever I've needed it, mere words cannot express how important that has been.

This work was supported financially by the Technical Development Foundation and the Gustav Komppa Fund of the Alfred Korelin Foundation.

LIST OF ORIGINAL PUBLICATIONS

This work is based on the following original publications which are referred to in the text only by their corresponding Roman numerals. Additionally, some unpublished data are presented and discussed.

I A. Niskanen, A. Rahtu, T. Sajavaara, K. Arstila, M. Ritala and M. Leskelä: Radical Enhanced Atomic Layer Deposition of Metallic Copper Thin Films, *J. Electrochem. Soc.*, **152** (2005) G25

II A. Niskanen, T. Hatanpää, K. Arstila, M. Leskelä and M. Ritala: Radical Enhanced Atomic Layer Deposition of Metallic Silver Films, submitted to *J. Mater. Chem.*, 2006

III A. Niskanen, K. Arstila, M. Ritala and M. Leskelä: Low Temperature Deposition of Aluminum Oxide by Radical Enhanced Atomic Layer Deposition, *J. Electrochem. Soc.*, **152** (2005) F90

IV A. Niskanen, K. Arstila, M. Leskelä and M. Ritala: Radical Enhanced Atomic Layer Deposition of Titanium Dioxide, submitted to *Chem. Vapor. Deposition*, 2006

V A. Niskanen, U. Kreissig, M. Leskelä and M. Ritala: Radical Enhanced Atomic Layer Deposition of Tantalum Oxide, submitted to *Chem. Mater.*, 2006

OTHER PUBLICATIONS BY THE SAME AUTHOR

Related to the current field of study

Mikko Ritala, Marianna Kemell, Markus Lautala, Antti Niskanen, Markku Leskelä and Sven G. Lindfors: Rapid Coating of Three Dimensional Through-Porous Substrates by Atomic Layer Deposition, accepted for publication in *Chem. Vap. Deposition*, 2006

Other publications

J. Molarius, T. Laurila, T. Riekkinen, K. Zeng, A. Niskanen, M. Leskelä, I. Suni and J. K. Kivilahti: Reactively Sputtered Ta_2N and TaN Diffusion Barriers for Copper Metallization, *AMC 2000 Proceedings*

H. Kattelus, J. Koskenala, A. Nurmela and A. Niskanen: Stress Control of Sputter-Deposited Mo-N Films for Micromechanical Applications, *MAM 2001 Proceedings*

A. Niskanen, T. Hatanpää, M. Ritala and M. Leskelä: Thermogravimetric Study of Volatile Precursors for Chemical Thin Film Deposition: Estimation of Vapor Pressures and Source Temperatures, *J. Thermal Anal. Calorim.*, **64** (2001) 955-964

K. Kukli, K. Forsgren, J. Aarik, T. Uustare, A. Aidla, A. Niskanen, M. Ritala, M, Leskelä and A. Hårsta: Atomic Layer Deposition Of Zirconium Oxide From Zirconium Tetraiodide, Water and Hydrogen Peroxide, *J. Cryst. Growth*, **231** (2001) 262-272

J. Raula, J. Shan, M. Nuopponen, A. Niskanen, J. Hua, E. Kauppinen and H. Tenhu: Synthesis of Gold Nanoparticles Grafted with a Thermo-Responsive Polymer by Surface-Induced Reversible-Addition-Fragmentetion Chain Transfer Polymerisation, *Langmuir*, **19(8)** (2003) 3499

J. Jernstöm, U. Vuorinen, M. Hakanen and A. Niskanen: Solubility of Thorium Under Anoxic Conditions, *Radiochem.*, 43 (2001) 465-470

K. Krogars, J. Heinämäki, M. Karjalainen, A. Niskanen, M. Leskelä and J. Yliruusi: Enhanced Stability of Rubbery Amylose-Rish Maize Starch Films Plasticized With A Combination of Sorbitol and Glycerol, *Int. J. Pharm.*, 251 (2003) 205-208

LIST OF ABBREVIATIONS AND ACRONYMS USED

AC	Alternating current
acac	2,4-pentanedionate (acetylacetonate)
ALD	Atomic Layer Deposition (also known previously as ALE, Atomic Layer Epitaxy)
Cp	Cyclopentadienyl, -C_5H_5
CVD	Chemical Vapour Deposition
DC	Direct current
EDX	Energy dispersive X-ray spectroscopy
Et	ethyl, -C_2H_5
FESEM	Field emission scanning electron microscope
MW	Microwave
PEALD	Plasma Enhanced Atomic Layer Deposition
Piv	pivalate, $(CH_3)_3CCO_2$-
PVD	Physical Vapour Deposition
REALD	Radical Enhanced Atomic Layer Deposition
RF	Radio frequency
O^{i}Pr	isopropoxide, -$OCH(CH_3)_2$
SEM	Scanning electron microscopy, scanning electron microscope
thd	2,2,6,6-tetramethyl-3,5-heptanedionate
TOF-ERDA	Time-of-flight elastic recoil detection analysis
UHV	Ultra high vacuum
XRD	X-ray diffraction
XRR	X-ray reflectivity

CONTENTS

1. INTRODUCTION

Atomic layer deposition (ALD) is a chemical thin film deposition method operating in vacuum (1). Significant early development for ALD was done under the name Atomic Layer Epitaxy (ALE) with the desire to manufacture thin film electroluminescent (EL) displays. Later, materials deposited by ALD found other applications such as solar cells, microelectronics, gas sensors, optics, and protective coatings. One of the key strengths of ALD is its capability to deposit conformal coatings with uniform thickness on even the most demanding topologies. This property has lead to ALD being used in the most demanding applications such as coating of nanometre scale structures like catalytic particles and microelectromechanical systems (MEMS) (2).

A vast majority of ALD processes published to date use two reactants at an elevated temperature to facilitate film growth. These kinds of processes are thus thermally activated. The thermally activated processes are often limited to operate at temperatures above 150 – 200 °C, as their feasibility is hindered by slow reactions at lower temperatures. Finding suitable reactants for the thermally activated growth of elemental materials such as metals is another challenge. In some cases, such as the ALD of silver and gold, finding a suitable metal precursor may already be challenging. If one is found, a compatible reducing agent is also needed for the reduction of the metal precursor to its elemental state.

In this thesis, the use of radicals as the second reactant is studied in the deposition of selected materials by ALD. The materials include two metals, copper (I) and silver (II), and three oxides, aluminium oxide (III), titanium dioxide (IV) and tantalum oxide (V). Hydrogen radicals were used as the second reactant in the deposition of metals, and oxygen radicals in the deposition of oxides. The metal precursors chosen for this work were widely used in thermal ALD and thus the film properties obtained by radical enhanced atomic layer deposition (REALD) could be compared to the results published for the thermal ALD

processes. The deposition of silver is an exception to this as the material has not been previously deposited by ALD before.

A brief review of the deposited materials is presented, along with some background on the generation of radicals by using plasmas. The reactor used in the experiments and its development is also described. The results are presented briefly, and will be discussed and summarized. Also, some unpublished data is presented and discussed. Finally, a conclusion about the suitability of radicals in ALD is given.

2. BACKGROUND

2.1 Plasma: generation, properties and reactions

Plasma is commonly considered as the fourth state of matter. The description arises from the fact that plasma may be obtained by heating a gas, like heating a solid produces liquid and heating a liquid produces gas. The description is somewhat misleading, because the transition between gas and plasma is gradual instead of the sharp transition between the more common phases: the amount of ionized gas simply increases with increasing temperature. Also, the above description implies that plasmas are always hot. Naturally, plasmas generated by heating a gas i.e. thermal plasmas are hot, but plasmas generated by electric fields may also be cold (3).

In thermal plasmas, the electrons, ions and neutral species are in local thermodynamic equilibrium. This means that the species in the plasma have for example the same average kinetic energy. In "cold" or non-equilibrium plasmas, the charged species are more energetic than the neutrals and light particles more than the heavy. As only a small part of the species in the plasma have a high energy, the overall temperature of the plasma is low, and hence the name. A cold, non-equilibrium plasma can be generated for example by applying an

alternating electric field between two parallel electrodes. The alternating electric field accelerates the few electrons present in the gas, either generated by cosmic rays or field emission from walls in confined plasmas. The accelerated free electrons undergo elastic and inelastic collisions with the gas molecules. The electrons do not lose, however, much of their energy mainly because of the large mass difference of the colliding bodies. This way, the electrons gain energy up to the point where they are able to excite or ionize molecules present in the gas. Ionization generates further electrons which are also accelerated by the electric field, and a dynamic, steady-state plasma discharge is generated. In the dynamic steady-state, the plasma continuously gains and loses charged species at equal rates, but is not in thermodynamic equilibrium (4). The above breakdown mechanism is called the radio frequency (RF-) breakdown, and may be obtained with high frequency alternating electric fields. Plasma can also be generated by direct current (DC) and lower frequency alternating electric fields. There, the breakdown is different: in particular, the electron losses on surfaces are more dominant than in the high frequency RF-breakdown (4).

In practice, laboratory plasmas are always confined. In confined plasmas ions, electrons and excited species are lost in collisions with surfaces, such as walls. As the surfaces are hit by electrons, the surface is charged negatively. Electrons dominate the charging process as they have much higher kinetic energy than positively charged species and thus hit the surfaces more frequently. The negative charge build-up continues until the surfaces repulse electrons strongly enough to result in equilibrium. Additionally, the negatively charged walls attract positive ions. The positive ions are accelerated towards the walls which in turn decreases the charging as the ions are lost. The overall effect of the negative charging is the acceleration of positive ions and a decrease in the electron losses.

There are many possible processes that can occur in a plasma (Table I), but in the scope of this work, the most important are the generation and elimination of the chemically active species and energetic ions. These are formed by dissociation, excitation and ionization when plasma electrons collide with gas

molecules. Radicals and ions are generated only when a colliding electron has sufficient energy to break chemical bonds or ionize the molecule. Both radicals and ions can be used in for example thin film research: radicals as highly reactive reactants and ions to produce physical changes in a sample. Ions recombine rapidly and are present in large quantities only inside the plasma discharge. Radicals are eliminated through a process called recombination. When using diatomic gases, radical recombination occurs only in the presence of three bodies due to the requirement for momentum conservation. The simultaneous collisions of three bodies at low gas pressure are however quite rare. As a result, the recombination proceeds often more rapidly on solid surfaces, as the surface serves as the third party and a collision of only two species is required. The recombination of polyatomic radicals is simpler as they may recombine in two body collisions where the momentum is transferred to bond vibrations. Radicals are longer lived than ions and are also present outside the plasma discharge region. With simple alterations to the experimental setup, it is possible to have either both energetic ions and radicals, or just radicals present on a sample. These two represent different cases in thin film processing, and the distinction between them is made in chapters 2.2.1 and 2.2.2, when discussing Plasma and Radical Enhanced Atomic Layer Deposition.

Table I. Some possible gas phase processes in a plasma discharge (3-5). A and B are reactants; A^+ and A^- are ions of A; A* is A in an excited state; e^- is an electron and hν is a photon with a specific energy.

Process	Reaction
Excitation	$A + e^- \rightarrow A^* + e^-$
Excitation	$A^+ + B \rightarrow A^+ + B^*$
Ionization	$A + e^- \rightarrow A^+ + 2\ e^-$, or $A_2 + e^- \rightarrow A_2^+ + 2\ e^-$
Ionization	$A^+ + B \rightarrow A^+ + B^+ + e^-$
Penning ionization	$A + B^* \rightarrow A^+ + B + e^-$
Dissociation	$A_2 + e^- \rightarrow 2\ A + 2\ e^-$
Dissociative attachment	$A_2 + e^- \rightarrow A + A^-$
Surface recombination	$A_{ads}^* + A_{ads}^* \rightarrow A_2$

Surface recombination	$e^- + A_{ads}^+ \rightarrow A$
Volume recombination	$e^- + A^+ + B \rightarrow A + B$
Volume recombination	$A^* + A^* + A_2 \rightarrow 2\ A_2$
Photoemission	$A^* \rightarrow A + h\nu$

Photoemission is a common process in plasmas, and produces a characteristic light emission from each excited species. In other words, discharges in different gases produce different colours. Light emitting plasma discharges are commonly referred to as glow discharges.

It is highly unfeasible to generate a plasma by heating gas, and therefore in a laboratory environment plasmas are generated and maintained by plasma sources (6). Probably most convenient is to use plasma sources based on electric fields. These plasma sources utilize either direct current (DC) or alternating current (AC). Either current mode can be used to generate plasma simply by applying a voltage between two parallel electrodes. In theory, plasma can be generated at all gas pressures, but in practice, the majority plasmas used in thin film deposition are low pressure plasmas. Plasma generation at higher pressures is more difficult, and achieving the same degree of ionization requires more energy due to the greater number of atoms and molecules present.

DC discharges are commonly used in fluorescent lamps. Plasma sources using alternating current are, however, more frequently used in deposition and process environments, as they are more versatile (3). The most common AC plasma sources are radio frequency (RF) and microwave (MW) plasma sources, most commonly operating at 13.56 MHz and 2.45 GHz. Plasmas generated by these sources are commonly referred to as electrical, gaseous or glow discharges.

As mentioned before, plasmas produce radicals and energetic ions. Radicals are used due to their high reactivity and energetic ions because they can produce

physical changes by momentum transfer. For example, as plasma is ignited in hydrogen gas the following dissociation process may occur:

$$H_2(g) + e^- \rightarrow 2\ H^{\cdot}(g) + e^-$$

Thus, two hydrogen radicals are produced from one diatomic hydrogen gas molecule, and the colliding electron loses some of its energy in the process. The reverse process is slow and the recombination proceeds more readily on solid surfaces than in the gas phase. Naturally, radicals can be generated from molecular oxygen (O_2) and nitrogen (N_2), or from compounds: dissociating ammonia (NH_3) results in a mixture of nitrogen and hydrogen radicals. Such a mixture of radicals may be used when both reduction and nitridation are required, such as in the deposition of transition metal nitrides (7-9). Similarly, hydrogen radicals are used when reduction is required, and oxygen radicals for oxidation (Tables II and IV). Some established commercial processes utilizing plasmas are the plasma enhanced chemical vapour deposition (PECVD) of silicon nitride and silicon oxide (5,10).

Sputtering is a process where energetic ions are used to remove atoms from a surface. This process can be used either for etching or material deposition. In sputter deposition, the surface from where the atoms are removed is called the target. The target is electrically biased to further accelerate ions towards it. As the accelerated ions hit the target material, the momentum transfer process ejects atoms from the target. The ejected atoms travel in the gas phase and condense as they hit a solid surface, including the substrate, and form a thin film of the target material. Even complex compounds can be sputter deposited by using multiple targets or a single target, provided it is homogeneous (11). Sputter deposition belongs to the physical vapour deposition (PVD) methods. In sputter etching, the ejected atoms are not collected and the target is the sample to be etched. By adding a suitable etching gas to the plasma chamber the etching speed can be enhanced or the etching process made selective (12). This modification is called reactive ion etching (RIE) (13).

2.2 Atomic Layer Deposition

Atomic Layer Deposition (ALD) is a chemical gas phase thin film deposition method (1). It belongs to the group of Chemical Vapour Deposition (CVD) methods. A characteristic of this group is that the films are formed via chemical reactions as opposed to PVD methods where the films are formed mainly via physical material transport.

The film deposition by ALD occurs via alternating, self-limiting surface reactions. As a result of the self-limiting reactions, growth by ALD, or in the ALD mode, is saturative. This means that the film forming reactions proceed to completion, and then stop. Thus, each ALD cycle results in precisely the amount of material deposited regardless of the exposure once the saturation threshold is exceeded.

The concept of the ALD window can be used to describe the temperature dependent processes which may or may not lead to film growth in the ALD mode (Figure 1). Processes leading to non-saturative growth, with either too high or low growth rates, occur outside the ALD window. An increased growth rate may either result from precursor condensation at too low temperatures, or from precursor decomposition at too high temperatures. Alternatively, a decreased growth rate may be a result of incomplete reactions at the low temperature regime, or of precursor desorption at too high temperatures. In the ALD window, the growth rate may or may not be dependent on temperature, depending on the particular process. The growth in the ALD window is, however, always saturative.

The use of radicals in the deposition process can eliminate the regime of incomplete reactions, provided that the metal precursor adsorbs to the surface, since radicals are assumed to react very rapidly. Thus, the ALD window is extended to lower temperatures, down to the condensation limit of the metal precursor. An example of a process where activating the reactant dramatically enhances the deposition rate, or lowers the deposition temperature is the

deposition of aluminium oxide from trimethylaluminium (TMA, $Al(CH_3)_3$) and molecular oxygen (O_2). This process has not been reported in the literature. However, deposition with possibly a more favourable metal precursor, aluminium chloride ($AlCl_3$), requires over 600 °C (14). By dissociating the oxygen with a plasma discharge aluminium oxide growth with TMA as the aluminium precursor was obtained already at room temperature, 25 °C (III).

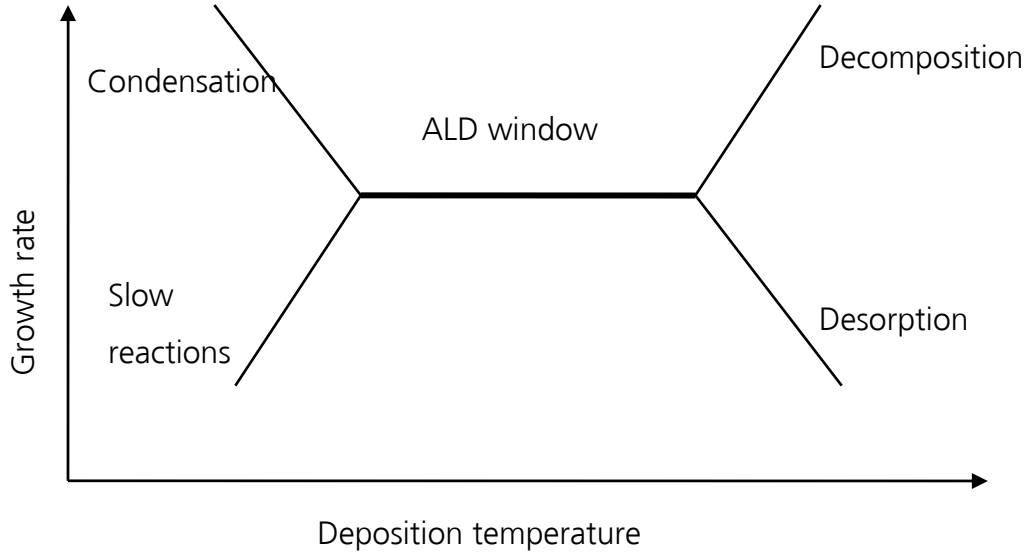

Figure 1. The ALD window, depicting the dependency of the growth rate on the deposition temperature. The temperature range resulting in ALD growth, i.e. the ALD window, is depicted with the bolded line. Condensation, decomposition, desorption and slow reactions are possible processes for a precursor outside the ALD window.

ALD processes have been studied and reviewed extensively (1,15). The material variety includes oxides, nitrides, sulphides, II-VI and III-V compounds, and elemental materials including both metals and non-metals.

The majority of the ALD processes studied to date are thermally activated. In thermally activated processes the reactants have their intrinsic reactivities towards the other reactant(s) and the overall kinetics can be sped up only by

increasing the deposition temperature. The main reasons that limit the deposition of certain materials with thermally activated ALD are that the metal precursor may decompose before sufficient reactivity is achieved, no reactivity between the reactants is achieved at all, and side- or etching reactions dominate. The deposition temperature may be further limited by the substrate, which may be a heat-sensitive material or a device structure. Low deposition temperature may also limit the obtainable film quality if the film forming reactions are slow or incomplete. For example, slow desorption of reaction by-products may result in increased amounts of impurities in the films. Some processes have demonstrated aggressive enough half-reactions and produced high quality films even at low temperatures (16), but others have suffered from excessively long cycle times and have shown high impurity contents (17).

2.2.1 Plasma Enhanced Atomic Layer Deposition

In PEALD, plasmas are used to dissociate gas to produce the desired radical, which then functions as the non-metal precursor. The metal precursor cannot be dissociated as this would lead to CVD growth. The distinctive feature of PEALD is that the substrate is located either inside the plasma discharge or very close to it, and is exposed to the charged species originating from the plasma (Figure 2, left). The proximity of the plasma discharge to the substrate results in a large flux of radicals which is a major advantage of PEALD. Also, the particle bombardment from the plasma may provide additional energy to the adsorbed species and increase their surface mobility and the rate of the film forming reactions. As a downside, the bombardment may result in surface damage and the close proximity of the plasma discharge can result in dissociation of possible reaction by-products or adsorbed precursors and thereby lead to contaminations (18). Also, the negative charging is present in PEALD on insulating surfaces. Thus, a risk of damaging insulating materials during deposition exists in PEALD as electrical breakdown may occur if the substrate holder for example is grounded. Most, if not all, PEALD reactors use an RF-

plasma source and operate at a few mbar pressure. The currently published PEALD processes are listed in Table II, and include mostly oxides but also some elemental materials and transition metal nitrides.

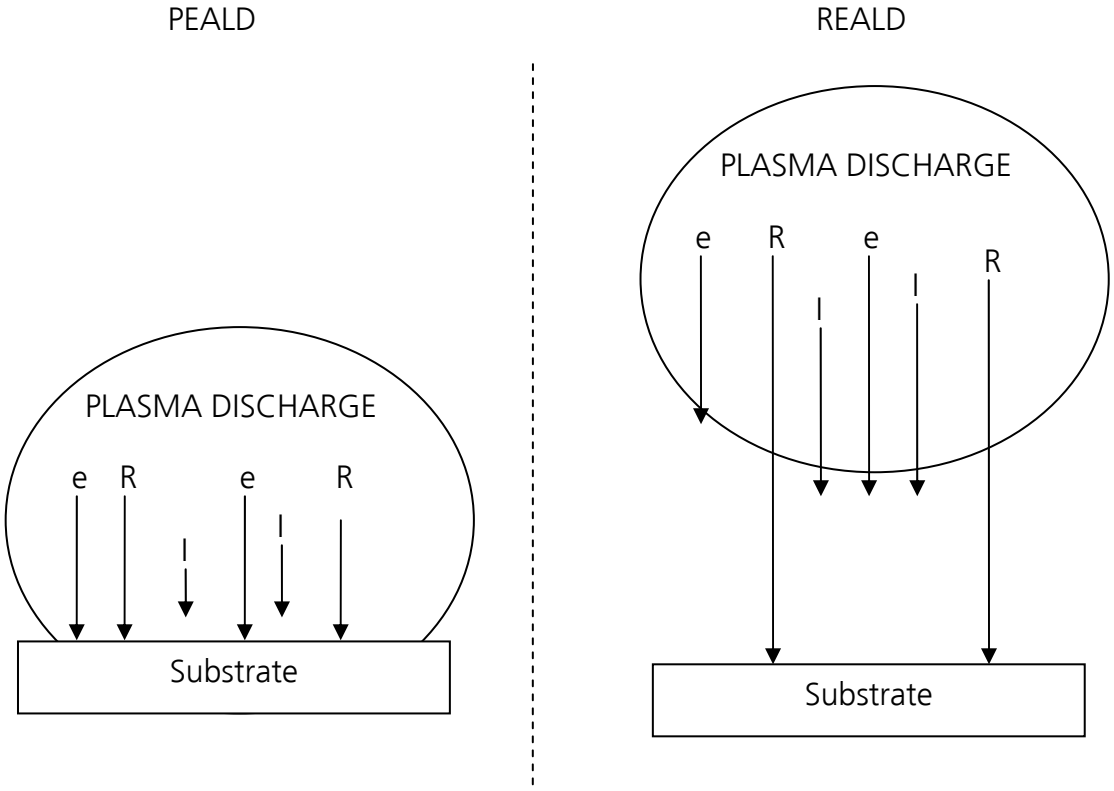

Figure 2. Schematic representations of how the plasma discharge is located with respect to the substrate in Plasma (left) and Radical Enhanced ALD (right). R is a radical, I is an ion and e is an electron.

Table II. Materials deposited by PEALD

Material	Metal precursor(s)	Dissociated gas	Deposition temperature / °C	Reference
Al	$Al(CH_3)_3$	H_2	250	(19)
AlN	$AlCl_3$	NH_3 and H_2	350	(7,8)
Al_2O_3	DMEAA	O_2	100 – 125	(20)
Al_2O_3	$Al(CH_3)_3$	O_2	200	(21,22)
Al_2O_3	$(CH_3)(C_4H_8)NAlH_3$	O_2	100	(23)

Al_2O_3	$Al(CH_3)_3$	O_2 and N_2	100 – 350	(24-26)
Al_2O_3:N	$Al(CH_3)_3$	O_2 and N_2	80	(27)
$AlSi_xO_y$	$Al(CH_3)_3$ and TEOS	O_2	120 – 150	(28,29)
Co	$CoCp(CO)_2$, $CoCp_2$	NH_3	300	(30)
Cu	$Cu(thd)_2$	H_2	180	(31)
Ga_2O_3	$[(CH_3)_2GaNH_2]_3$	O_2	200	(32)
HfO_2	$Hf[OC(CH_3)_3]_4$	O_2	100	(33)
HfO_2	$Hf(NEt_2)_4$	O_2	250	(34,35)
HfO_2	$Hf(NEt_2)_4$	N_2O	340	(36)
Ni	$NiCp_2$	H_2	165	(37)
Ru	$Ru(EtCp)_2$	NH_3	270	(38,39)
Ru-TiN	$Ru(EtCp)_2$, $Ti[N(CH_3)_2]_4$	N_2, H_2 and N_2	200	(40)
$SrTiO_3$	$Sr(thd)_2$, $Ti(O^iPr)_4$	O_2	250 – 350	(41)
$SrTa_2O_6$	$Sr[Ta(OEt)_5dmae)]_2$	O_2	300	(42)
TaN	$(EtN)_3Ta{=}NC(CH_3)_3$	H_2	260	(43,44)
Ta(N)	$Ta[N(CH_3)_2]_5$	He and H_2	275	(45)
Ta_2O_5	$Ta(OEt)_5$	O_2	280	(46)
Ta_2O_5	$Ta[N(CH_3)_2]_5$	O_2	250	(47)
Ti_xAl_yN	$Ti[N(CH_3)_2]_4$, $Al(CH_3)_3$	NH_3[a], H_2	180	(48)
Ti_xAl_yN	$TiCl_4$, $AlCl_3$	H_2 and N_2, H_2 and NH_3	350	(49)
TiN	$Ti[N(CH_3)_2]_4$	H_2 and/or N_2	175	(50)
TiN	$TiCl_4$	H_2 and N_2	270 – 370, 100 – 400	(51,52)
TiO_2	$Ti(O^iPr)_4$	O_2	200	(53)
TiO_2	$Ti(O^iPr)_4$	O_2 and N_2	250	(54)
TiO_2	$Ti[N(CH_3)_2]_4$	O_2	200	55
TiO_2	$Ti[N(CH_3)_2]_4$	O_2	200	(47)

Ti_xSi_yN	$TiCl_4$, SiH_4	H_2 and N_2	350	(56)
WC	$W[N(CH_3)_2]_2[N=C(CH_3)_3]_2$	H_2 and N_2	250	(57)
ZrO2	$Zr[NEt_2]_4$ or $Zr[OC(CH_3)_3]_4$	O_2	250	(58)
ZrO_2	$Zr[OC(CH_3)_3]_4$	O_2	100	(33)
ZrO_2	$Zr[N(Et)(CH_3)]_4$	O_2	110 – 250	(59,60)

[a] unactivated NH_3 used to deposit TiN

2.2.2 Radical Enhanced Atomic Layer Deposition

In REALD, only radicals are let to reach the substrates. This is realized by placing the substrates in a remote location with respect to the plasma source (Figure 2, right), which results in the elimination of energetic ion and electron bombardment on the substrates. The film forming reactions are thus governed by the radicals' chemical behaviour. Also, as the substrates are not exposed to ion or electron bombardment, no additional energy is provided in the film forming reactions. Thus, the rate of the film forming reactions is determined by the reactivities of the used precursors and by-product desorption at the prevailing temperature, like in thermal ALD. On the other hand, the possibility for surface damage and precursor decomposition is decreased. The radicals may also be formed by other means, for example hydrogen radicals can be generated by thermal cracking with a heated tungsten filament.

As radicals recombine on a surface very rapidly, saturative adsorption is not observed, like with metal containing precursors. Film growth in the ALD mode should still be obtained if the reactions that radicals undergo with the adsorbed metal precursor do proceed to completion. As with any new ALD process, the growth rate saturation as a function of pulse length must be demonstrated for both precursors. Additionally, good conformality should also be shown for each new REALD process, but keeping in mind that the radical depletion due to recombination may be severe in structures with very small dimensions.

As radicals are somewhat different from the more commonly used non-metal precursors, it may be worthwhile to examine how they fulfil the requirements set for ALD precursors (1) (Table III).

Table III. Requirements for ALD precursors (after reference 1, with permission).

Requirement	Comments
Volatility	For efficient transportation, a rough limit of 0.1 Torr at the applicable maximum source temperature Preferably liquids of gases
No self-decomposition	Would destroy the self-limiting film growth mechanism
Aggressive and complete reactions	Ensure fast completion of the surface reactions and thereby short cycle times Lead to high film purity No problems of gas phase reactions
No etching of the films or the substrate material	No competing reaction pathways Would prevent the film growth
No dissolution into the film or the substrate	Would destroy the self-limiting film growth mechanism
Unreactive volatile by-products	To avoid corrosion
Sufficient purity	To meet the requirements specific to each process
Inexpensive Easy to synthesize and handle Non-toxic and environmentally friendly	

The requirement for sufficient volatility can be understood as a requirement to obtain the desired reactant in sufficient amounts. This can be fulfilled by a proper reactor design and sufficient pulse lengths. The requirement for no self-decomposition means that the precursor should not decompose in a way that

leads into a solid deposit. Radicals do not decompose, but are lost through recombination, which results in no additional growth, only in the loss of reactants. In this respect, the requirement is fulfilled, but the loss of radicals may lead to issues with up-scaling the deposition process to large substrates. The radicals undergo fast reactions and thus fulfil the requirement for aggressive and complete reactions. The highest risk of etching the substrate or the deposited film occurs when the substrates are exposed to the plasma discharge. In REALD this possibility should be eliminated since a remote, downstream plasma configuration is used. The formation of hydrogen chloride may be a cause for film or substrate etching in some processes. This could occur, for example, when using metal halides and hydrogen radicals in the same process. Additionally, the formation of volatile species during the film deposition offers a distinct possibility for etching the film. Examples of such species are ruthenium tetroxide, RuO_4, which could be formed during the deposition of ruthenium oxide, and silane, SiH_4, during the deposition of silicon.

The requirement for no dissolution into the substrate or the growing film is fulfilled by the high reactivity of the radicals. As a result, the radicals may react with the substrate and are generally unable to penetrate materials due to reactions or recombination. Reactions with the substrate may result in the formation of hydrides, nitrides or oxides. An example of the oxide formation was seen in the ALD of aluminium oxide on silicon from trimethylaluminium and oxygen plasma, where a thin silicon oxide layer formed under the deposited film (21). A slightly thinner interfacial oxide layer was obtained with ozone as the oxygen source, and no interfacial oxide was seen when using water. In a related study, it was observed that the use of remote oxygen plasma, i.e. oxygen radicals, did not produce an interfacial layer at all (61). Apparently, the avoiding the formation of the interfacial oxide is very challenging since in another study even remote plasma formed such a layer (34,35,62). As the radicals used in a process contain only one or two elements, the risk of forming reactive or non-volatile by-products should be less than with thermally activated precursors. Additionally, the reaction by-products probably undergo further reactions with the radicals and reduce or oxidize to very simple compounds. The requirement

for sufficient purity is easily fulfilled as the purity depends on the used gases, which can be further purified if desired. Radicals are also non-toxic and environmentally friendly as they recombine very rapidly. The radicals, however, do not satisfy the requirements for inexpensiveness and ease of handling, due to the difficulty of generating the radicals in the first place and the relatively expensive equipment required. On the other hand, many of the precursors used to deposit noble metals do not fulfil the last two requirements either and are still considered quite successful processes (see Section 2.3).

The majority of REALD processes reported so far can be divided into two groups: processes done in ultra high vacuum (UHV), evacuation-type reactors, and processes done at a few mbar pressure with continuous flow reactors (1). Only recently two commercial REALD capable reactors were introduced: a travelling-wave reactor Ever-Tek Plus-200 (61), and an evacuation-type reactor FlexAL by Oxford Instruments. The majority of the published work was made using self-built reactors, mainly due to the brief availability of commercial reactors. The published REALD processes including the ones presented in the current work are outlined in Table IV.

Table IV. Materials deposited by REALD

Material	Metal precursor(s)	Dissociated gas	Deposition temperature / °C	Reactor type	Reference
Al_2O_3	$Al(CH_3)_3$	O_2	25 – 300	Flow	III
Al_2O_3	$Al(CH_3)_3$	O_2	300	Travel	(61)
Ag	$AgPiv(PEt_3)$	H_2	150	Flow	II
Cu	$Cu(acac)_2$	H_2	150 – 200	Flow	I
Er_2O_3	$Er(thd)_3$	O_2	200 – 300	UHV	(63)
HfO_2	$Hf(NEt_2)_4$	O_2	250	Flow[b]	(34,35,64)
HfO_2	$Hf(mp)_4$	O_2	250	Flow	(62)
Ge	Et_2GeH_2	H_2[a]	420 – 528	UHV[a]	(65,66)

Pd	$Pd(hfac)_2$	H_2	80	UHV	(67)
$SrTiO_3$	$Sr(thd)_2$ and $Ti(O^iPr)_4$	O_2	150 – 275	Flow	(68)
$SrTiO_3$	$Sr(thd)_2$ and $Ti(O^iPr)_4$	H_2O	250	Flow[b]	(69)
Ta	$TaCl_5$	H_2	25 – 400	UHV	(70-72)
TaN	$TaCl_5$	H_2 and N_2	300	UHV	(73,74)
TaN	$Ta[N(CH_3)_2]_5$	H_2 and/or N_2	250 – 300	UHV	(75)
Ta_2O_5	$Ta(OEt)_5$	O_2	150 – 300	Flow	V
Ti	$TiCl_4$	H_2	25 – 400	UHV	(70,76)
TiN	$TiCl_4$	H_2 and N_2	400	UHV	(77)
TiN	$TiCl_4$	D_2 and N_2	25 – 137	UHV	(78)
TiN	$Ti[N(CH_3)_2]_4$	N_2	150 – 350	Flow	(79)
TiN	$Ti[N(CH_3)_2]_4$	N_2 and/or H_2	250	Flow	(80)
TiN	$Ti[N(CH_3)_2]_4$	H_2 or N_2 or NH_3	250	Flow	(9)
TiO_2	$Ti(O^iPr)_4$	O_2	50 – 300	Flow	IV
Y_2O_3	$Y(thd)_3$	O_2	200 – 300	UHV	(81)
ZrO_2	$Zr(NEt_2)_4$	O_2	250	Flow	(82)

[a] dissociated with a tungsten filament

[b] uncertain

2.3 ALD of metals

The ALD of metals has always been quite challenging. To date, the following metals have been deposited either by using a thermally activated process or with additional activation: Al (19), Ti (70,76), Fe (83), Co (83), Ni (37,83,84), Cu (I, 31,83-90), Mo (91), Ru (38-40,92-96), Rh (97), Pd (67,94,98-100), Ta (70-72), W (101-104), Ir (105), and Pt (84,106).

The largest challenge in depositing metals with only thermal activation has been in finding an effective reducing agent. Metallic zinc is one, especially in the

deposition of transition metal nitrides (107,108), but the risk of zinc dissolution into silicon or the deposited materials themselves has limited the interest in it. Molecular hydrogen has been used widely, but it is not very active in its diatomic form and required an activating surface, metallic platinum or palladium, in the ALD of copper using CuCl and $Cu(thd)_2$ (86,87). Molecular hydrogen has also been used with transition metal amidinates to deposit Fe, Co, Ni and Cu films by thermal ALD (83). Amidinates seem like a potential precursor group for ALD of metals, especially as molecular hydrogen can be used without an activating surface. However, only limited film properties were reported and, consequently, further studies on the film properties are required before the suitability of amidinates as ALD precursors can be established. A fresh approach to ALD of metals has been reported with the deposition of noble metals. There, the ligand is decomposed oxidatively and at the same time the metal is reduced to its elemental state (93). Finally, tungsten has been deposited with thermal ALD from WF_6 and Si_2H_6 (101-104). Besides the above processes, the deposition of metallic films by ALD still remains as a challenge.

2.3.1 Copper

Copper has the second lowest resistivity of all metals. It recently replaced aluminium as the main conductor material in microelectronic circuits. An ALD copper process would seem to be applicable in depositing a thin seed layer of copper on which the commonly used electroplating process could be applied (109,110). The seed layer is required to promote adhesion to the diffusion barrier and guide the crystallographic texture of the electroplated copper (109). ALD could replace PVD as the seed layer deposition method, since the seed layer must be conformal on even the highest aspect ratio structures.

Copper has been deposited by thermal ALD (83-90), REALD (I) and PEALD (31). The processes have used copper β-diketonates (I,84,87-89), CuCl (85,86,90,111) or copper dialkylacetamidinato (83) as the metal containing precursor. The reducing agents have been molecular hydrogen (83,84,86,87,90),

zinc vapour (85), alcohols or formaldehyde (88,89). Copper has also been grown epitaxially by ALD on (001) α-Al_2O_3 from CuCl and a mixture of H_2O and H_2 at 400 °C (111). A common feature of the thermally activated processes is that the reducing agent is less than optimal. Probably the most suitable reducing agent for any deposition process would be atomic hydrogen. Its advantages are high reducing power, reactivity and chemical compatibility with most processes. The main limitation for using atomic hydrogen is that it needs to be produced *in-situ*, by for example dissociating molecular hydrogen with a plasma source or a hot tungsten filament.

Copper deposition using PEALD was also reported (31). The process was based on $Cu(thd)_2$ and atomic hydrogen generated by an inductively coupled RF-plasma plasma source. Copper has also been deposited via reduction of CuO: first a CuO layer was grown by thermal ALD which was then reduced to metallic copper with organic molecules such as alcohols, aldehydes or formic acid (112).

2.3.2 Silver

Silver has the lowest electrical resistivity, 1.59 $\mu\Omega$cm, of the known, non-superconducting materials, and the highest thermal conductivity. Because of the lower resistivity, silver may be the only replacement for copper in integrated circuits, especially as its resistivity in under 100 nm features was reported to be much less than that of Cu (113-117).

Silver is also a highly reflective material, and thus has a low emissivity, and is therefore a very good choice if reflectivity in the IR region is also needed (118). For these reasons silver is being used in mirrors where the highest obtainable reflectivity is required. The high reflectivity has resulted in silver being used as a decorative material in utensils, i.e. as silverware, and in jewellery. Additionally, thin silver films have been used as gas sensors, where gases chemisorbing on the silver surface change its reflectivity (119). Silver surfaces are also good partial oxidation catalysts, and are used to catalyse several reactions: oxidative

coupling of methane (CH_4) (120), partial dehydrogenation of methanol (CH_3OH) into formaldehyde (121), and the partial oxidation (or epoxidation) of ethylene (C_2H_4) (122).

Monolayers of silver have been used as surfactants in the deposition of giant magnetoresistive (GMR) spin valves (123,124). The structure generally consists of a magnetic transition metal layer, such as Co, Ni or Fe, and a layer of some noble metal, such as Au, Ag or Cu. The use of a surfactant reduces the agglomeration of the transition metals when they are deposited on the noble metals. As a result, the interfaces are smoother and the layers in the GMR structure better defined. The surfactant floats out during the deposition of the transition metal, which is promoted in the case of silver by its large atomic volume. An order of magnitude increase in was reported in the GMR properties of a NiO-Co-Cu-Co structure with the incorporation of the silver surfactant into the manufacturing process (124).

The REALD of silver (II) is the first reported ALD process for the material as no reference to a successful deposition of silver by ALD was found in the literature. This is probably due to a lack of a suitable silver precursor, reducing agent and a lack of interest in the ALD of silver. Silver films have been deposited with both CVD (125,126), and PVD methods such as evaporation and sputtering.

2.4 ALD of oxides

Oxides are probably the most studied materials in the field of ALD research. The deposition of oxides by ALD has been reviewed extensively by Ritala and Leskelä (1), and Puurunen (15). Generally, the most common metal precursors are halides, alkoxides and alkyls. The thermally activated oxide processes have widely used water as the oxygen-containing precursor. Also other oxygen sources, such as H_2O_2, O_3 and metal alkoxides, have been used. In the following chapters the applications and deposition of aluminium oxide (Al_2O_3), titanium dioxide (TiO_2) and tantalum oxide (Ta_2O_5) are reviewed briefly.

2.4.1 Aluminium oxide

Aluminium oxide has suitable properties for many applications. As thin films, Al_2O_3 can be used as a dielectric, passivating and protecting material. It has a moderately high dielectric constant (κ = 9), and a high electric field strength. Aluminium oxide also has a high band-gap, 8.7 eV. These properties make it an attractive material for gate dielectric in metal-oxide-semiconductor (MOS) transistors.

The thermally activated ALD of aluminium oxide has been studied very widely, and thus only a few representative references are listed below. For a more comprehensive discussion on the subject, see the review by Ritala and Leskelä (1) or by Puurunen (15). The most common aluminium containing precursors have been $AlCl_3$ (127-129) and $Al(CH_3)_3$ (TMA) (17,21,130-136). Some studies have also been made with alkoxides $Al(OEt)_3$ and $Al(O^nPr)_3$ (137), and $Al(CH_3)_2(O^iPr)$ (138). Also the use of an alkyl-halide precursor $Al(CH_3)_2Cl$ has been studied (139). Water is the most commonly used oxygen source (17,21,127,130-133,136,138), but also ozone (21,134,135), alcohols (137), and aluminium alkoxides (140) have been used.

Aluminium oxide has been deposited with REALD from TMA and oxygen radicals (III). The deposition with PEALD has been studied with more precursor combinations: TMA and O_2 (21,22), TMA and O_2-N_2 mixture (24-26), DMEAA and O_2 (20), and methylpyrrolidine alane ($(CH_3)(C_4H_8)NAlH_3$, MPA) and O_2 (23).

2.4.2 Titanium dioxide

Titanium dioxide has a range of attractive properties which make it suitable for many thin film applications. Titanium dioxide has a high refractive index, 2.2 - 2.6 depending on the deposition method and thus the film structure, and can be thus used for optical coatings (141,142). It also has a high dielectric constant, 80 – 110, which makes it an interesting candidate for high-κ gate dielectrics

(143). The major limitation in this application is that titanium dioxide suffers from high leakage currents. Recently, titanium dioxide has received wide attention as a bioactive (144) and photocatalytic material (145,146).

Titanium dioxide has been deposited by thermally activated ALD from titanium halides and alkoxides: $TiCl_4$ (142,147-158), TiI_4 (159-163), $Ti(O^iPr)_4$ (IV,54,164-167), $Ti(OEt)_4$ (168-171) and $Ti(OMe)_4$ (145). The oxygen-containing precursors have been water (142,145,147-152,154-159,164-166,168-171), hydrogen peroxide (159,160,166), molecular oxygen (161,162) and ozone (167). Titanium dioxide has also been deposited by REALD and PEALD from $Ti(O^iPr)_4$ and oxygen radicals (IV,53,54), and $Ti[N(CH_3)_2]_4$ and O_2 plasma (172).

2.4.3 Tantalum oxide

Tantalum oxide is very stable chemically and thermally, and has suitable properties for protective, optic, optoelectronic and electronic applications. Tantalum oxide has a moderately high dielectric constant: 22 – 28 for amorphous and up to 40 for the crystalline phase (173,174). Despite the high leakage currents that tantalum oxide generally suffers from, it is relatively easy to integrate into existing manufacturing processes. Thus, tantalum oxide is being used in integrated thin film capacitors and as a dielectric layer in ultra large scale integration (ULSI) dynamic random access memory (DRAM) devices. Tantalum oxide films have been used as protective coatings on, for example, solid state electrochromic devices (175).

Tantalum oxide has been deposited by thermally activated ALD using several different tantalum precursors: $TaCl_5$ (176-179), TaI_5 (180), $Ta(OEt)_5$ (129,181,182), and alkylamides (183). Oxygen containing precursors have been water (176-183), hydrogen peroxide (180) and oxygen (184). An interesting process was reported by Kukli *et al.* where they deposited tantalum oxide by the reaction between $TaCl_5$ and $Ta(OEt)_5$ (185).

Tantalum oxide has also been deposited by photoassisted ALD from $Ta(OEt)_5$ and water (186), $Ta(OEt)_5$ and O_2 (187) and by REALD and PEALD using $Ta(OEt)_5$ and oxygen radicals (V,46). Finally, *in-situ* reaction mechanism studies were made by Kukli *et al.* where they studied the thermally activated deposition of tantalum oxide from $Ta(OEt)_5$ and H_2O between 70 and 375 °C (182). Rahtu *et al.* used mass spectrometry to study the reaction mechanisms of the thermally activated ALD of tantalum oxide from $Ta(OEt)_5$ and D_2O (169).

3. EXPERIMENTAL

In this chapter, the experimental details are described. More specific information about the processes can be found in the corresponding publications and from the cited references.

3.1 Reactor design for Radical Enhanced Atomic Layer Deposition

As there were no commercially available reactors for REALD, one had to be constructed in this work. To have the possibility to use low-vapour pressure solid precursors, an existing flow-type ALD reactor, the F-120 by ASM Microchemistry, was chosen as the starting point for constructing the REALD reactor. This reactor has a well working solid precursor feed system operated with inert-gas valving (1). An open chamber version of the reactor was used instead of the more widely used compact quartz cassette, to which it would have been very difficult to incorporate the radical source.

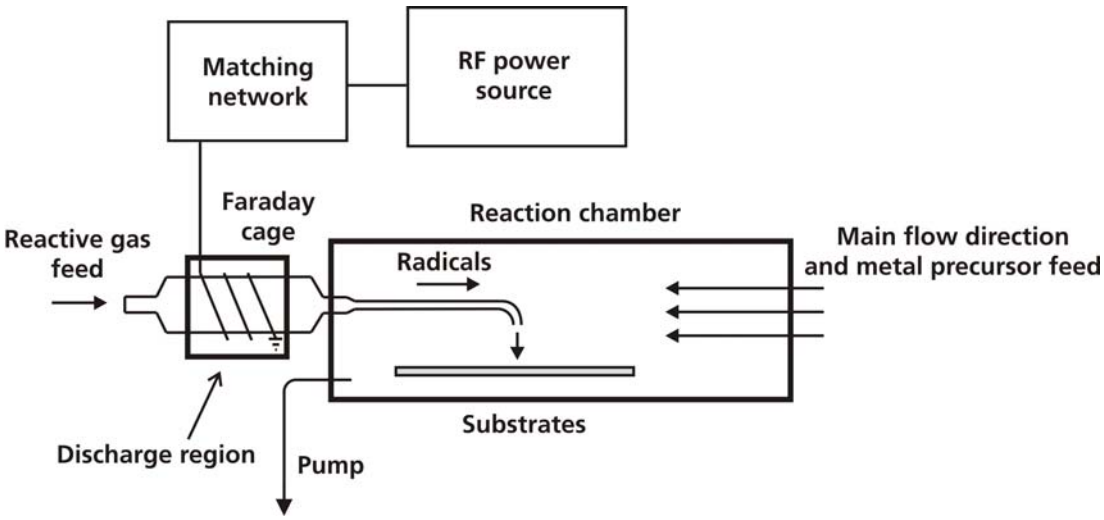

Figure 3. A schematic drawing of the RF-REALD reactor. Reactor components are not in scale.

Several types of plasma sources would theoretically be suitable for REALD. A capacitively coupled RF-plasma source was considered first, but for some reason the ignition of plasma was not successful with this setup. As a result, inductive coupling was used in the first RF-plasma ALD reactor (Figure 3). However, due to several reasons, the RF-source was changed into another plasma source.

First, in the chosen reactor, heating coils surround the substrate area. Therefore the RF-coil needed to be located outside the reactor volume, as the electric field generated by the RF-coil could easily induce into the heating coils and further to the electronics of the reactor. For the same reason, the heating coils themselves could not be used to generate the electric field. Furthermore, using the heating coils would have possibly resulted in the generation of plasma in the deposition chamber and PEALD-like situation. The discharge region and the induction coils could not be located inside the reactor because having two concentric vacuum tubes with different gases in them could lead to a situation where the plasma is ignited in an unwanted area, i.e. between the tubes.

Second, in the chosen reactor the distance between the substrates and either end of the reactor is long. Because the plasma source needed to be located

outside the reactor, the radicals have to travel a long distance to reach the substrates. And finally, the operation of the RF-plasma source proved to be unreliable in the reactor as the gas pressure inside the reactor changed constantly. As a result, the plasma discharge failed frequently to ignite, making the estimation of actual deposition cycle amount impossible.

For these reasons, a surface-wave (SW) launcher plasma source, powered with a microwave source, Sairem GMP 03KE/D with IC 336, and launched by Sairem SURF451 surfatron (188,189) was installed into the reactor (Figure 4). The main advantages of the SW launcher are its small size, it is relatively easy to operate and, most importantly, the discharge can be made to extend very close to the substrates (188). This will help to minimize recombination, because radicals are generated all the way to the substrates. Such a long extension would not have been possible with the RF-plasma source. The SW launcher generates a travelling electromagnetic wave onto the inner surface of the discharge tube. The travelling wave, in turn, generates radicals as long as it has sufficient energy to do so.

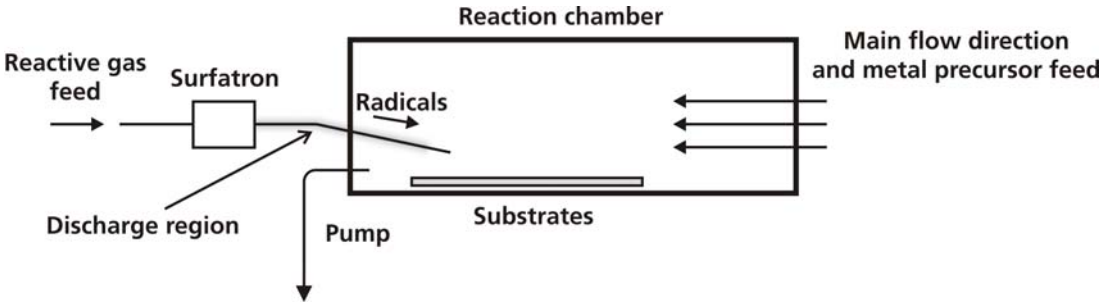

Figure 4. A schematic drawing of the final REALD reactor, using a microwave plasma source.

The plasma column was chosen to extend very close to the substrates, yet still leaving them downstream of the discharge. This way, the substrates are protected from particle bombardment and charged species. The radicals are generated in the discharge tube made of glass or quartz from the desired gas. The tube passes through the surfatron SW launcher, into the ALD reactor, and onto the substrates (Figure 5). The length of the plasma column is adjusted by

both power setting and the flow rates of gases running through the discharge tube. Increasing the power setting increases the surface-wave energy, and if a fixed gas flow is used, the length of the discharge column is increased. With a fixed power, the column length is a result of the balance between radical production and recombination as a function of pressure. Therefore, there is an optimum in flow rate which maximizes the discharge column length.

Several other considerations needed to be made due to the unique nature of the plasma source. The electromagnetic field launched by the surfatron is easily reflected by conductive materials. This is a result of the field extending radially outside the discharge tube (188). As the plasma is generated by the electromagnetic field, it is desirable to allow it to travel as unhindered as possible. Consequently, most metallic parts surrounding the path of the discharge tube were substituted with plastic ones. Polycarbonate was chosen as the replacement material, as it is very stiff, can withstand moderately high temperatures, and is transparent. Later, it was seen that polycarbonate withstood plasma damage much better than Teflon. When in contact with plasma, polycarbonate was consumed very uniformly, whereas channels traversing the entire object were rapidly produced in Teflon.

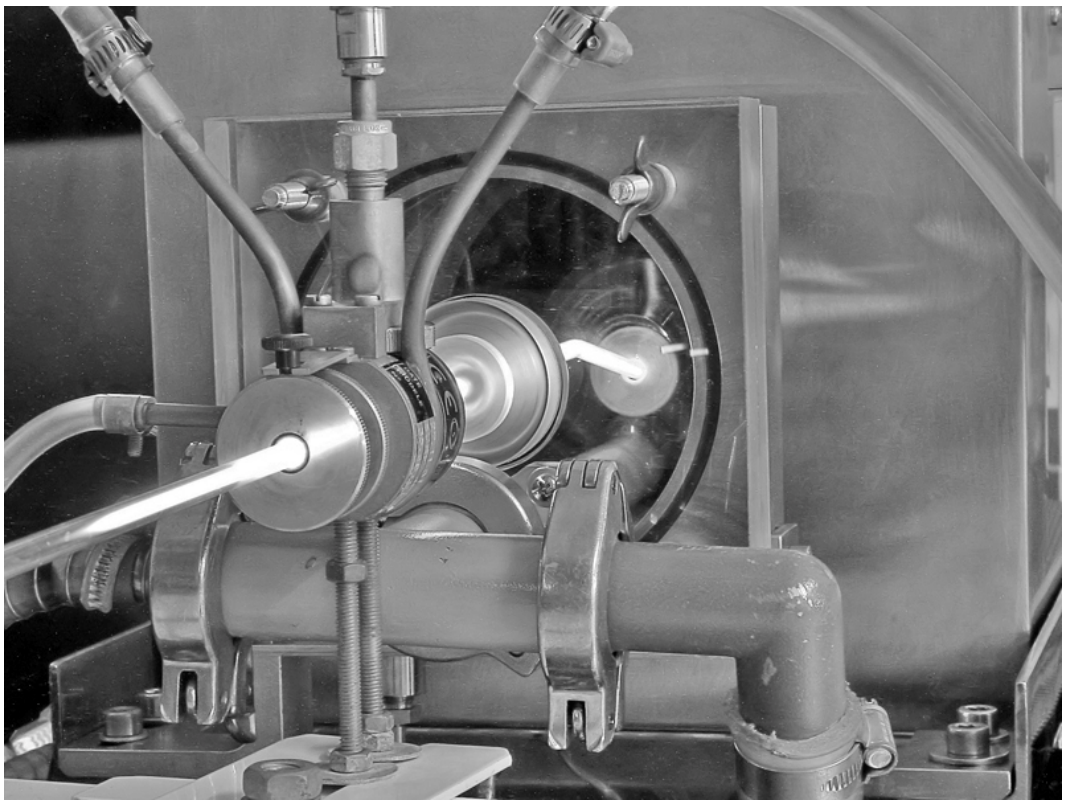

Figure 5. A photograph of the REALD reactor viewed from the plasma source end. The plasma source is operated at full power. The discharge tube enters the reaction chamber through the light grey disc.

The substrates are located in an open volume in the REALD reactor. This volume was minimized to speed up pulsing and purging. Argon was used as the carrier and purge gas in the REALD reactor. More commonly used nitrogen could not be used, since it is dissociated by the plasma discharge into radicals with unwanted reactivity. Argon and hydrogen were purified with point of use gas purifiers, as even trace amounts of oxygen could lead to oxygen radicals and oxidation when depositing metals.

3.2 Film deposition

The films were deposited using the REALD reactor described in chapter 3.1. A typical REALD deposition cycle is outlined in Table V.

Table V. A typical REALD deposition cycle with the range of pulse and purge times and plasma power used

Step	1	2	3	4
Action	Metal precursor pulse	purge	Reactive gas pulse	purge
Time / s	0.2 – 5	0.2 – 10	4 – 12	3
Plasma power / W (%)	20 (7)	20 (7)	300 (100)	20 (7)
Discharge flow / sccm	0	0	60	0

The simultaneous pulsing of the discharge flow and plasma power was necessary to sustain the plasma discharge throughout the film growth process. Sustaining the plasma discharge is crucial, since the ignition of plasma is not simple with this type of plasma source. During each radical pulse two 3 second periods were required to increase and decrease the plasma power in a controlled fashion to avoid the accidental extinguishing of the plasma discharge. The discharge flow contained the desired reactive gas mixed with argon. The reactive gas was either hydrogen or oxygen, to deposit either metals (I, II) or oxides (III–V). The amount of reactive gas mixed with argon was set by using the maximum power for the plasma and adjusting the amount of reactive gas to produce a discharge column with the optimal length.

Most films were deposited on 5x5 cm^2 glass substrates and silicon (I–V). While film growth was observed on the entire substrate area, the saturated growth was observed as a circle of uniform thickness. The circle increased in diameter as the radical pulse was lengthened, and eventually covered the entire substrate area. The deposition temperatures were limited by the condensation of the

metal precursor, its thermal decomposition, and the reactor's material restrictions. For example, $Cu(acac)_2$ begins to decompose at about 250 °C (84), which is thus the highest temperature at which it may be used in ALD. The thermal decomposition for TMA does not begin at least until 375 °C (190), but the materials used in the REALD reactor limit the highest possible deposition temperature to 300 °C.

3.3 Film characterization

The films were characterized with several methods. Film crystallinities were studied with grazing incidence x-ray diffraction (GIXRD) (I–V). X-ray reflectivity (XRR) was used to measure the film thickness, density and surface roughness (I,III–V). XRR was limited to films with less than 150 nm thickness and 6 nm roughness on the top surface. Both GIXRD and XRR measurements were conducted with a Bruker-AXS D8 Advance x-ray diffractometer/reflectometer operating in parallel beam geometry. For over 80 nm thick transparent films, the thicknesses and refractive indices were determined by fitting optical transmittance or reflectance spectra measured within a wavelength range of 370-1100 nm using a Hitachi U-2000 Spectrophotometer (191) (III–V). Energy dispersive X-ray analysis (EDX) was used to measure the film thicknesses from the rough, non-transparent films, which could not be analyzed by XRR (II). The EDX measurements were analyzed with the GMR electron probe thin film program (192). The EDX measurements were conducted with an INCA Energy 350 spectrophotometer connected to a Hitachi S-4800 field emission scanning electron microscope (FESEM) (II). Additionally, atomic force microscopy (AFM) measurements conducted with a ThermoMicroscopes CP Research instrument were used to measure the surface roughness and verify the results obtained by XRR (I). The X-ray crystal structure of the precursor synthesized for the ALD of silver was determined with a Bruker Nonius KappaCCD diffractometer using graphite monochromated Mo$K\alpha$ radiation (II).

The film conformality was studied by cross-sectional SEM measured with a Hitachi S-4800 field emission scanning electron microscope (FESEM) (II,IV-V), and a Jeol JSM-7400F Electron Microscope (I). The presence of aluminium oxide deposited at low temperatures on polymers and natural fibres was verified by scanning electron microscopy (SEM) using a Zeiss DSM-962 electron microscope, and energy dispersive x-ray spectroscopy (EDX) using a Link ISIS spectrometer (III). Also, the penetration titanium dioxide into the wool fibre was studied by the Hitachi FESEM, and EDX mapping using the INCA Energy 350 spectrophotometer (IV).

Sheet resistances of the conductive films were measured with the four-point probe technique using a Keithley 2400 SourceMeter with an Alessi C4S Four Point Probe head (I,II). The leakage currents of the dielectric films were analyzed using a metal-insulator-metal (MIM) structure. The films were deposited on a conductive sputter deposited indium tin oxide (In_2O_3:Sn, ITO) (III) or evaporated platinum (IV,V). Aluminium dots were evaporated with an Edwards Auto 306 resistive evaporator through a shadow mask to form the top electrodes (IV,V). The platinum (III–V) and some aluminium (III) evaporation was done with an Instrumentti Mattila IM-1992 electron beam evaporator.

The Keithley 2400 SourceMeter was also used for measuring the leakage current densities (III–V). Capacitance measurements were done with a HP4284A LCR meter using measuring frequencies of 10 to 100 kHz (III–V). The breakdown voltage and dielectric constant were measured from several electrodes and the reported values were obtained from at least three electrodes.

Film impurity contents were analyzed by time-of-flight elastic recoil detection analysis (TOF-ERDA) (193) (I–V). Fourier-transform infrared spectroscopy (FTIR) performed with a Perkin Elmer Spectrum GX spectrophotometer in transmission mode was used to study the aluminium oxide phases and the chemical nature of the impurities (III,IV).

The photocatalytic activity of the crystalline titanium dioxide films was studied by decomposing methylene blue in an aqueous solution under UV irradiation (145), using a General Electric F20T12/BLB 20 W black light blue fluorescent lamp which has the main emission at 365 nm (IV).

4. RESULTS AND DISCUSSION

The results reported in this chapter are presented in more detail in references I–V. Here, the results are reviewed and discussed with the emphasis on how changing the non-metal precursor to radicals affects the growth and film properties. Also, results from unpublished experiments are summarized. Most of the unpublished experiments were done during the survey of suitable processes to be studied with REALD. The most successful ones were chosen to be studied further in this thesis, but some of the successful ones may have potential to be working ALD processes.

4.1 Metals

Both copper and silver were deposited using hydrogen radicals as the reducing agent. The metal-containing precursors were, however, quite different. Whereas the copper process utilized a readily available commercial precursor, the silver precursor was synthesized in-house.

4.1.1 Copper (I)

The REALD of copper was done with copper(II)2,4-pentanedione ($Cu(acac)_2$), and hydrogen radicals (I). The deposition temperature was chosen as low as possible. As the evaporation temperature of $Cu(acac)_2$ was 125 °C, the lowest feasible deposition temperature which did not cause condensation of the copper precursor in the deposition zone was 140 °C. The growth, however,

occurred at least up to 200 °C. The saturated growth rate for copper was found to be 0.018 nm per one ALD cycle, with a 1 second $Cu(acac)_2$ pulse and 5 second hydrogen radical pulse. The purge periods after these pulses were 4 and 3 seconds. As the overall cycle time was 13 seconds, a 0.08 nm/min growth was thus obtained. Higher growth rates of 0.2 nm/cycle (89) and 0.04 nm/cycle (83) have been reported in the literature for thermal ALD of copper. Comparing these results to the REALD of copper is difficult, since both precursors in the thermally activated processes were chemically different. The films were polycrystalline on both silicon and glass substrates, and exhibited both (111) and (200) XRD reflections. The RMS roughness values measured by XRR and AFM were in the range of 2 – 3 nm for about 25 nm thick films, which is lower than what has been reported earlier for copper films deposited by thermally activated ALD.(90) The film adhesion was studied by the Scotch tape peel test, and the films were found to be adherent on silicon, HF-etched silicon, glass, SiLK (194, a low dielectric constant organic polymer for replacing silicon dioxide), evaporated copper, and ALD grown TaN (195) and TiN (196) films.

Saturated surface reactions should also result in conformal film growth. This was verified with cross-sectional SEM images from a film deposited on a patterned trench substrate (Figure 6). As can be seen from the image, the film thickness is equal on the bottom and the top surface, which shows that the hydrogen radicals did reach the bottom of the trench. Together, growth rate saturation and conformality prove that the film growth does occur in the ALD mode.

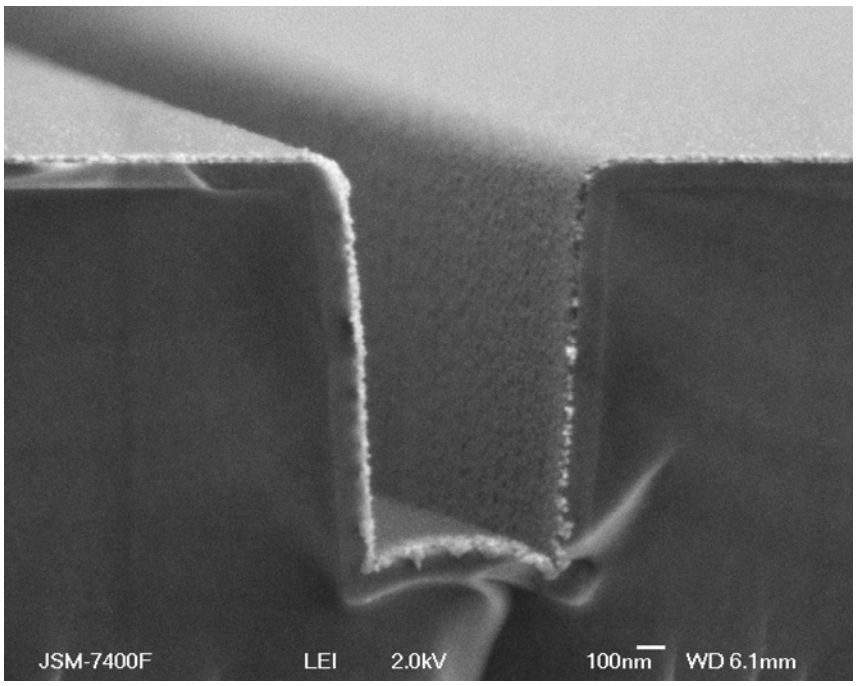

Figure 6. An SEM image of a 30 nm thick copper film deposited on a 2:1 aspect ratio trench.

Film purity was studied with and without argon and hydrogen purification. The copper films grown with the gas purification contained approximately 11-at.% oxygen, 2-at.% hydrogen and 1-at.% carbon as analyzed by TOF-ERDA, whereas the films grown without gas purification contained approximately 12-at.% oxygen, 8-at.% hydrogen and 5-at.% carbon. The values are quite similar, but some additional contamination seems to arise from the use of less pure gases. It can be concluded that the process seemed to tolerate trace amounts of water and/or oxygen and still form conductive copper. In both cases, the desorption rates of oxygen and hydrogen during the TOF-ERDA measurement lead to the assumption that some oxygen was in the form of an adsorbed water layer. As the measurements were done *ex-situ*, the films were exposed to air prior to the measurement. This is the most likely source of the adsorbed water. Interestingly, the use of gas purification resulted in significantly lower $Cu(acac)_2$ usage. One explanation for this could be that the $Cu(acac)_2$ reacts with trace moisture from the carrier gas to form $Cu(acac)_2 \cdot xH_2O$ and evaporates more rapidly.

The film resistivity was quite low, 15 μΩcm for a 25 nm thick film. The film thickness, grain size, surface roughness and impurity contents all increase the lowest obtainable resistivity (197). Based on the contribution of thickness alone, the theoretical minimum for resistivity for a 25 nm thick Cu film is approximately 6 μΩcm. The grain size and surface roughness in the film were approximately 23 and 3 nm. Taking these into account increases the lowest obtainable resistivity to close to the observed resistivity, making the contribution of film impurities very small or negligible. Mårtensson *et al.* obtained higher resistivity values with the thermally activated $Cu(thd)_2$ + H_2 process (87). They found that the resistivity increased with decreasing film thickness, a common phenomenon in thin metal films (198,199), and was 41.2 μΩcm for a 40.9 nm thick film.

Jezewski *et al.* deposited copper films with PEALD (31). They used $Cu(thd)_2$ and hydrogen radicals at 180 °C deposition temperature. Although deposition at 90 °C was reported, it is doubtful that the deposition is ALD-like, because the evaporation temperature of $Cu(thd)_2$ was 123.5 °C and precursor condensation occurs very likely below this temperature. The growth rate was 0.011 nm/cycle on SiO_2, and 0.020 nm/cycle on TaN_x and Au. These values are similar to the growth rate obtained with the REALD Cu process. The films were less rough than the REALD Cu films of similar thickness: only 0.4 nm RMS roughness was measured for a 24.5 nm thick PEALD Cu film deposited on SiO_2. The smaller roughness obtained with PEALD may be caused by the use of a slightly different copper precursor or a smoothening effect caused by the plasma's particle bombardment (18). Another alternative is that they have used crystalline SiO_2, or quartz, substrates whereas the REALD depositions were conducted on borosilicate glass. The PEALD process produced adherent films, as studied by the Scotch tape peel test. The film crystallinity was also studied with selected area electron diffraction (SAED). The films were reported to be polycrystalline with a (111) preferred orientation. The film composition was studied with Rutherford backscattering spectroscopy (RBS) *ex-situ* from films deposited on a 40 nm thick tantalum sputtered on an amorphous carbon wafer. The PEALD Cu

films contained 58 atom-% Cu, 32 atom-% O, 1-3 atom-% C and 9 atom-% Si. The oxygen contents are significantly higher than what was obtained for the REALD Cu films. If only due to air exposure, the oxygen contents should be comparable since both measurements were conducted *ex-situ*. Especially, as the REALD films were exposed to air for approximately two weeks prior the TOF-ERD analysis. The carbon contents were very similar for the PEALD and REALD films. The silicon impurities observed in the PEALD deposited films were not, however, seen in the REALD films. Thus, the authors' explanation of the plasma dislodging silicon atoms from the used equipment seems plausible. Finally, the resistivities of the PEALD films were not reported; the authors only commented that the films were conductive.

4.1.2 Silver (II)

The deposition of silver by ALD is demonstrated for the first time. Whereas an inexpensive, commercially available precursor was used for the REALD of copper, the silver films were deposited using in-house synthesized (2,2-dimethylpropionato)silver(I)triethylphosphine, $Ag(O_2C^tBu)(PEt_3)$, (Figure 7). The precursor forms trimeric chainlike aggregates where one carboxyl ligand acts as a bridging ligand. The precursor was evaporated at 125 °C, which should eliminate the possibility of decomposition, as a normal pressure thermogravimetric (TG) analysis under N_2 revealed that the compound decomposes in one step at 200-280 °C. The deposition sequence was like with copper, and similarly the deposition temperature was chosen as low as possible. The films were successfully deposited on silicon and glass. A saturated growth of 0.12 nm/cycle was obtained at 140 °C using a 3 second silver precursor pulse and a 7 second hydrogen radical pulse. The silver precursor was purged for a period of double the pulse length. Insufficient purging resulted in a massive increase in the film resistivity. The growth obtained in one minute was 0.51 nm. The growth rate is much higher than with the REALD copper (I), which produced only 0.018 nm/cycle or 0.08 nm/min. The difference in the growth rates is possibly due to the different metal precursors used in the processes (I,II).

If the silver precursor adsorbs as a trimer it may lead to higher growth rate as there are three silver atoms delivered to the surface per one adsorbed precursor molecule whereas only one is delivered by $Cu(acac)_2$.

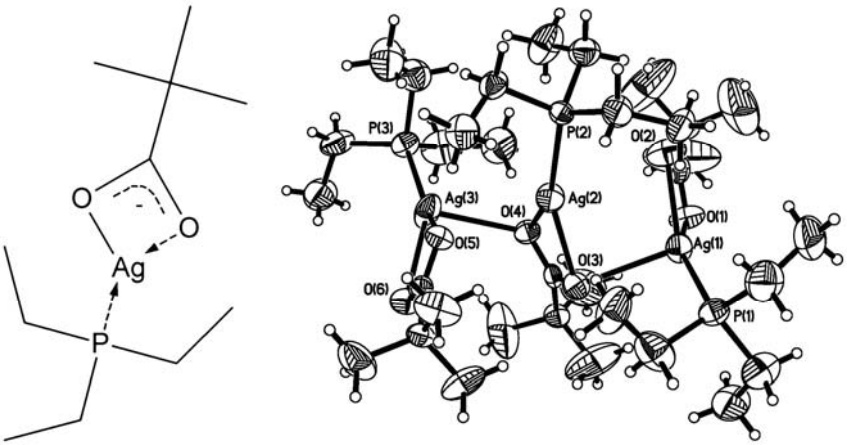

Figure 7. **Left:** The molecular structure of $Ag(O_2C^tBu)(PEt_3)$.
Right: The crystal structure of $Ag(O_2C^tBu)(PEt_3)$. A single asymmetric unit is shown, with the thermal ellipsoids drawn on 50 % probability level.

The films were polycrystalline and as a result, very rough. The film thicknesses could thus not be analyzed by XRR, but instead EDX measurements were used. The high roughness can also be seen in the SEM image (Figure 8), which also shows that the films grew conformally despite the high roughness. Visually the films were, however, mirror-like. The films were also relatively pure, containing only 4.0 atom-% phosphorous, 5.0 atom-% hydrogen and 1.0 atom-% carbon. The purity is also evident in the low film resistivity, only 6 μΩcm for a 40 nm thick film. Again, the film thickness, grain size and surface roughness increase the lowest obtainable resistivity value (197-199). The effect of surface roughness alone is expected to be significant as the films are very rough. Therefore, with the addition of the grain size effect, the contribution of the impurities may be very small. The low resistivity also verifies that the films are continuous even on a macroscopic scale. The film purity was better than for the REALD copper (I). The difference may well be a result of a more favourable

chemistry in the ligand removal, or simply of the less reactive nature of silver, as it is less electropositive than copper.

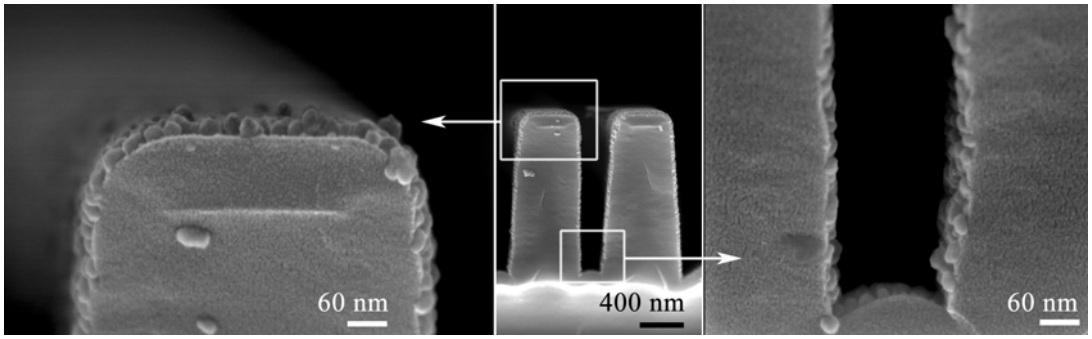

Figure 8. A cross-sectional SEM image of a 40 nm thick silver film deposited on a patterned trench substrate.
Left: A close-up of the top of a trench
Middle: An overview of the trench substrate
Right: A close-up of the bottom of a trench

4.1.3 Other experiments

The deposition of the following metals and nitrides (Table VI) were attempted but no growth or formation of an oxide resulted. Most of the metal precursors are known to adsorb on the used substrates, as the deposition of other materials has been successful with them. No growth suggests that either there is no reaction between the metal precursors and hydrogen radicals, or no adsorption after one monolayer growth. However, as most of the materials listed in Table VI have been deposited by PEALD or UHV-REALD, a more plausible explanation for no growth is that the radical flux was not sufficient in our experiments. Additionally, the oxide formation may be a result of oxygen-containing residues in the carrier gas, as gas purification was not yet used during these experiments.

Table VI. Experimental parameters for unsuccessful metal and nitride experiments

Material / substrate	Metal precursor	Reactive gas	Temperature / °C	Result
TiN / Si	$TiCl_4$	N_2, N_2+H_2	300	No growth, only two experiments conducted
Al / Si, glass, Cu	$Al(CH_3)_3$, $Al(OEt)_3$, or $AlCl_3$	H_2	100 – 250, 200 100 - 200	No growth or oxide formation
AlN / Si, glass	$Al(CH_3)_3$	N_2	250	No growth
Ru / glass	$RuCp_2$	H_2	200	No growth
Ta / Si, glass	$TaCl_5$	H_2	130 - 200	No growth
Nb / Si, glass	$Nb(OEt)_5$	H_2	150	No growth
Hf / Si, glass	$HfCl_4$, or HfI_4	H_2	200, 150 - 200	No growth
Cr / Si, glass	$Cr(acac)_3$	H_2	160 - 250	No growth
Mo / Si, glass	$MoCl_5$	H_2	150	No growth
Ni / Si, glass	$Ni(O^iPrN(CH_3)_2)_2$	H_2	100	No growth

4.2 Oxides

The oxide films were deposited using oxygen radicals as the oxygen source. The aim with the oxide films was to study metal precursors used in existing thermal ALD oxide processes and see how using oxygen radicals as the oxygen source affects the film properties. Also, decreasing the deposition temperature compared to the existing processes was attempted, followed by the deposition on heat sensitive materials. The literature is reviewed with respect to how altering the oxygen source affects the film growth and properties.

4.2.1 Aluminium oxide (III)

Aluminium oxide was deposited from TMA and oxygen radicals by REALD between 25 and 300 °C (III). The saturated growth rates were 0.31, 0.23, 0.23 and 0.15 nm/cycle for films deposited at 25, 100, 200, and 300 °C (Figure 9, left). The growth rate thus decreased with increasing temperature. The growth rate saturation required approximately 10 s cycle time, the growth rates as nanometres per minute were 1.8 and 0.9 nm/min for films deposited at 25 and 300 °C. In addition to silicon, glass and evaporated platinum, the deposition experiments at room temperature were conducted on polyethene, paper and wool. The successful deposition on especially wool is encouraging, since it serves to demonstrate the gentleness of the REALD process. In a related study in our laboratory, an identical wool fibre was exposed directly to low-power oxygen plasma and was oxidized (burned) within seconds.

The film densities increased with increasing deposition temperature from 2.52 to 2.76, 2.94 and 3.73 g/cm^3, for films deposited at 25, 100, 200 and 300 °C (Figure 9, left).

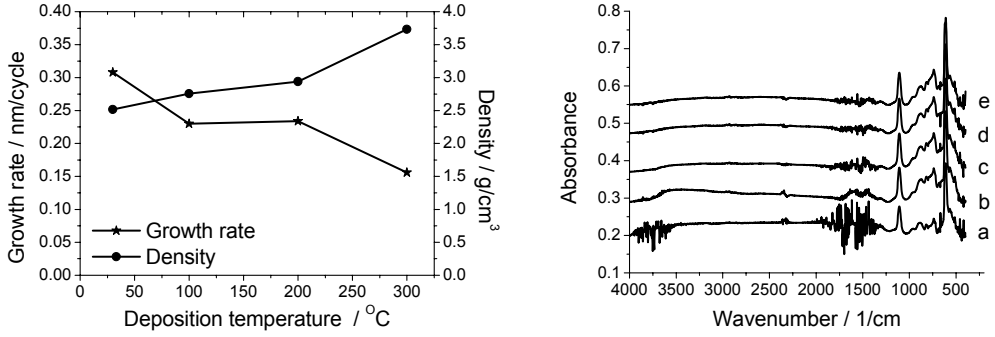

Figure 9. **Left:** The dependence of growth rate and density on the deposition temperature.

Right: Infrared absorption spectra of Al_2O_3 films grown using either H_2O (a) or O-radicals (b-e) as the oxygen precursor. The film deposition temperatures were 150 °C (a), 25 °C (b), 100 °C (c), 200 °C (d) and 300 °C (e).

The impurities in the films were analyzed by TOF-ERDA (Table VII). As a general trend, the impurity contents decreased with increasing deposition temperature. The films were very close to stoichiometric Al_2O_3 at 300 °C deposition temperature. At 25 °C deposition temperature the film composition is closer to AlOOH. In the films deposited above 100 °C, the impurities seem to appear with a 1:3 C:H –ratio, which suggests that the impurities are residual methyl groups from TMA (Table VII). Based on the FTIR-measurements (Figure 9, right), however, all samples were similar, even the one grown at 25 °C. The films contained only features associated to Al_2O_3 and not to AlOOH, for which an Al=O stretch should be seen in the IR spectrum at 1067 or 1022 cm^{-1} for crystalline and amorphous forms (200). The only difference between the samples is in the intensity of the very broad AlO-H stretch between 2600 and 3800 cm^{-1} (130) which increases with decreasing deposition temperature. Thus, as the sample grown at 300 °C is nearly pure Al_2O_3 (Table VII) and the sample grown at 25 °C displays similar FTIR spectrum, the latter seems to be Al_2O_3 also. Thus, the hydrogen seems to be in the form of residual methyl or hydroxyl groups instead of a discrete AlOOH phase. Finally, the refractive indices were between 1.60 and 1.64 at 580 nm wavelength for samples grown at 25 and 300 °C. The increasing values are in accordance with the increasing film density and purity.

The leakage current behaviour was also quite consistent with the impurity contents of the films: the leakage current prior to catastrophic breakdown decreased with increasing deposition temperature, and was negligible for films deposited at over 200 °C. The catastrophic breakdown occurred at 8.1, 10.2, 9.2, and 9.9 MV/cm for films deposited at 25, 100, 200, and 300°C, and the leakage currents preceding the breakdown were 100, 2.4, 0.8, and 0.4 $\mu A/cm^2$. Interestingly, the dielectric constant was approximately 8 for TMA-water, PEALD and REALD deposited films regardless of the deposition temperature (II, 17,24).

Table VII. The composition of REALD Al_2O_3 films according to TOF-ERDA.

	The amount of an element present / atom-%			
Deposition temperature / °C	Al	O	H	C
25	25	56	15	3.8
100	32	58	7.8	2.3
200	38	59	2.5	1
300	40	59	0.8	0.15
Stoichiometric Al_2O_3	40	60	0	0

Groner *et al.* studied the deposition of aluminium oxide from TMA and water at both low (17), and more typical higher temperatures (133). They obtained growth rates of 0.111, 0.134 and 0.125 nm/cycle at 33, 125 and 177 °C. These are lower growth rates than what was obtained with REALD. They obtained almost identical film densities as compared to REALD films at 33 and 177 °C, 2.46 and 3.06 g/cm^3. The hydrogen contents in the films according to forward recoil spectrometry (FReS) were and 22 and 7 atom-% at 33 and 177 °C deposition temperatures. These are higher than obtained with the REALD process at similar temperatures. Thus, at least compared to this case, changing the oxygen source from water to oxygen radicals decreased the hydrogen content in the films. The higher hydrogen content of the TMA-water process is reflected also in the refractive indices which were 1.51 and 1.60 for films deposited at 33 and 177 °C. The differences in the reported values may partly be explained by the differences in measuring the refractive indices, but overall the values obtained from the REALD films are higher. Groner *et al.* also measured the leakage current behaviour, and the catastrophic breakdown occurred at 3.7 and 4.4 MV/cm for films deposited at 33 and 177 °C. Here, the REALD films clearly outperform the thermally deposited ones. A major difference between the room temperature REALD and the thermal TMA-water ALD process is in the cycle times. The cycle time for the thermally activated process at 33 °C was 203 s and for the REALD process at 25 °C it was 10 s. The long cycle time is a result of the very slow purging water at low temperatures.

Kim *et al.* studied the deposition of aluminium oxide from TMA and ozone (134,135). They obtained a 0.085 nm/cycle growth rate at 380 °C deposition temperature. This is lower compared to both thermally activated TMA-water process and the REALD process. They obtained conformal growth and low impurity contents, less than 1 atom-% of carbon according to AES depth profiling. The film stoichiometry was found to be $Al_{2.2}O_{2.8}$ by RBS analysis.

Ha *et al.* studied the deposition of aluminium oxide by using TMA and three different oxygen sources: water, ozone and oxygen plasma (21). They obtained a 0.08nm/cycle growth rate using water and a 0.06 nm/cycle rate using ozone, both at 350 °C. The growth rate with oxygen radicals was 0.14 nm/cycle at 200 °C. Lim *et al.* also obtained a high, 0.18 nm/cycle, growth rate with PEALD using TMA and O_2-N_2 gas mixture as the reactants (24). Lim *et al.* also studied the leakage current behaviour of the PEALD films and obtained results similar to REALD: the catastrophic breakdown occurred at approximately 9 MV/cm electric field for films deposited between 100 and 250 °C. It is, however, unclear how the incorporation of nitrogen affects the electrical properties of Al_2O_3 in this case.

The above studies depict a certain order between the growth rates using TMA with different oxygen sources: ozone seems to produce the lowest growth rates followed by water, and oxygen radicals seem to produce the highest growth rates. This order is further confirmed by Ha *et al.* in their comparative study (21). The growth rate differences may be explained by differences in the number of adsorption sites left on the surface by the difference oxygen sources: higher number of adsorption sites would lead to higher number of adsorbed metal precursor and thus to higher growth rate. Overall, using oxygen radicals as the oxygen source produced the highest quality films and thus seems the best suited of the reviewed oxygen sources for depositing aluminium oxide with TMA as the metal precursor. The suitability of oxygen radicals and the effects on the film properties may be different in the case of different aluminium precursors such as halides or alkoxides.

4.2.2 Titanium dioxide (IV)

Titanium dioxide films were deposited with REALD between 50 – 300 °C from titanium isopropoxide, $Ti(O^iPr)_4$ and oxygen radicals (IV). The saturated growth rate at 50 °C was 0.19 nm/cycle, obtained with a 0.2 second $Ti(O^iPr)_4$ and a 7 second oxygen radical pulse. As the overall cycle time was 11 seconds, the growth rate was 1.0 nm/min. Increasing the deposition temperature to 300 °C decreased the growth rate to 0.16 nm/cycle or 0.87 nm/min. Deposition in ALD mode was further verified by the conformal growth seen in the cross-sectional SEM image taken from a 30 nm thick titanium dioxide film deposited on a substrate with patterned trenches (Figure 11).

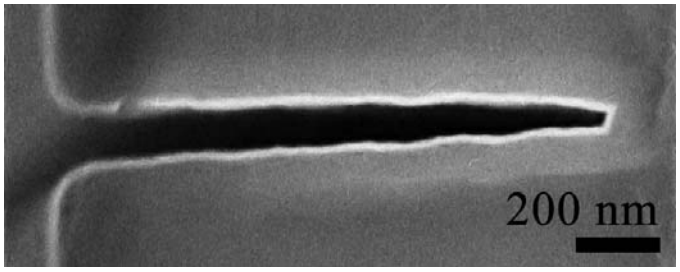

Figure 11. An SEM image of a 40 nm thick titanium dioxide film deposited onto a 10:1 aspect ratio trench. The image has been rotated 90 degrees counter-clockwise for convenience.

The film density was 3.2 – 3.4 g/cm^3 at 50 °C and increased to 3.8 g/cm^3 as the deposition temperature was increased to 250 °C. The surface roughness also increased with increasing deposition temperature, from 1.0 to 1.6 nm for 40 nm thick films deposited at 50 and 250 °C. This may indicate a beginning of crystallization, although the film grown at 250 °C was still amorphous according to XRD. Increasing the deposition temperature to 300 °C resulted in a very rough, crystalline film with the anatase phase. The film deposited at 50 °C had a titanium-oxygen ratio of 1:2.2 and contained 13 atom-% of hydrogen and 4 atom-% of carbon according to TOF-ERD analysis. The impurity contents decreased with increasing deposition temperature, and were only 0.5 atom-%

for hydrogen and 0.4 atom-% for carbon at 250 °C. The titanium-oxygen ratio also increased to nearly stoichiometric. The refractive indices at 580 nm were 2.2 and 2.4 for films grown at 50 and 300 °C. The crystalline film deposited at 300 °C was also tested for photocatalytic activity. The film, however, showed only very weak photocatalytic activity, especially when compared with the most active films deposited with thermal ALD from titanium methoxide and water (145).

The films grown between 50 and 300 °C with pulse lengths sufficient for growth rate saturation were insulating according to the four-point probe measurements. Some films deposited with insufficient oxygen radical pulses had a conductivity that was measurable by the four-point probe. Conductive, oxygen deficient TiO_2 was deposited by Ritala from $TiCl_4$ and water (201). A 58 nm thick film grown on platinum at 50 °C showed some dielectric properties, however. The dielectric constant of the film was 20. The electric field causing a 1 $\mu A/cm^2$ leakage current density was approximately 0.1 MV/cm (Figure 12). The catastrophic breakdown occurred at 0.63 MV/cm field. The catastrophic breakdown occurred at 0.67 MV/cm in a slightly thicker film deposited also at 50 °C.

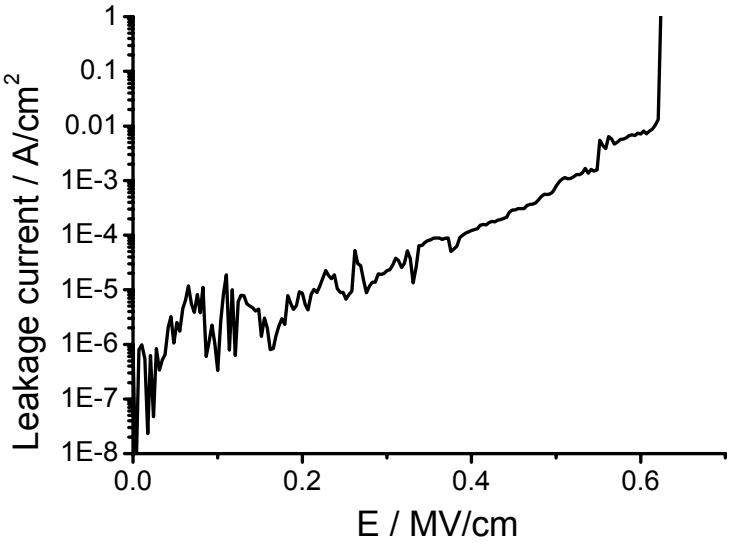

Figure 12. The leakage current as a function of applied electric field for a 58 nm thick TiO_2 film deposited on evaporated platinum.

The deposition on heat-sensitive substrates was studied at 50 °C. For these experiments, natural wool, polycarbonate, polypropene, polyethene and paper were used. The results were again very encouraging, as the deposition was successful on all the tested substrates without damaging them. This is demonstrated by the SEM images of the wool, where the original morphology of the wool fibre is visible even after the deposition (Figure 12). An EDX line scan taken from a cross-section of a single wool fibre coated with titanium dioxide (Figure 13) shows that the radicals have not damaged the fibre, by for example forming pores or channels, and titanium dioxide was deposited only on the surface of the fibre.

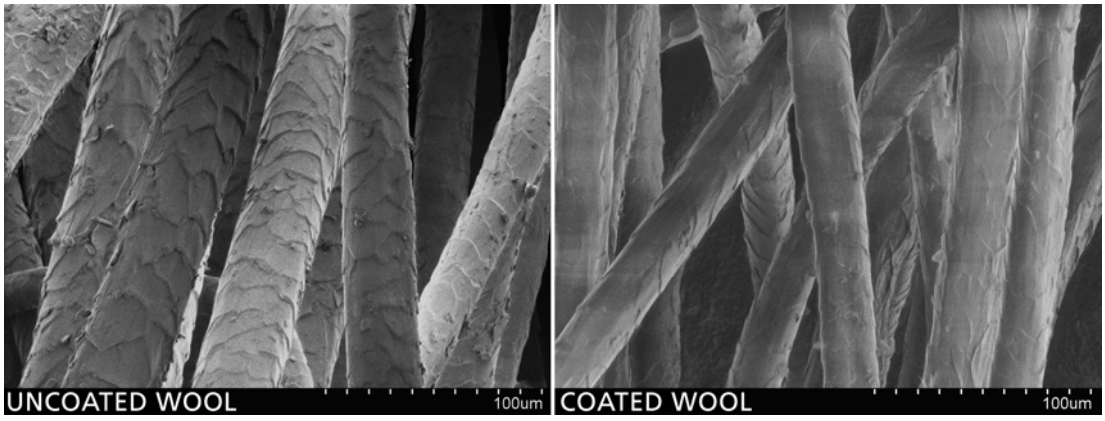

Figure 13. A scanning electron microscope image of a wool fibre coated with titanium dioxide (right). An uncoated wool fibre is displayed on the left.

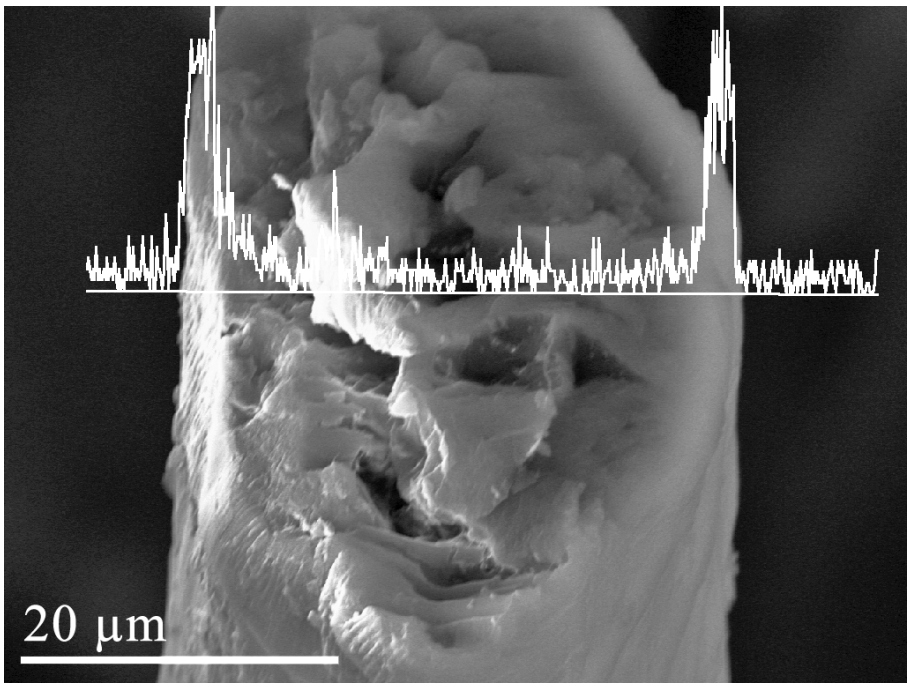

Figure 14. An energy dispersive x-ray spectroscopy line scan overlaid on a scanning electron microscope image of a wool fibre coated with titanium dioxide. The concentration of titanium was measured along the straight white line, which also functions as the baseline for the titanium concentration curve (displayed in arbitrary units).

The deposition of titanium dioxide with the thermally activated process from $Ti(O^iPr)_4$ and water has been studied by several authors (164-166). Ritala *et al.* obtained saturated growth with a 0.03 nm/cycle rate between 250 and 325 °C (164). The growth rate was found to increase to 0.06 nm/cycle with a higher water dose (165,166). By changing the oxygen source to the more oxidizing H_2O_2, Aarik *et al.* reported an increase in the growth rate, to 0.12 nm/cycle, though with a different reactor (166). Ritala *et al.* analyzed the film crystallinity by XRD and the films were found to be partly crystalline already at 250 °C. The crystallinity increased with the deposition temperature, which could be seen as the intensification of the anatase phase reflections. They observed a refractive index of 2.5 above 225 °C deposition temperature, and the value decreased slightly to 2.3 as the deposition temperature was decreased to 150 °C. The hydrogen content in the film bulk was 0.3 atom-% as analysed by NRA (164).

The carbon content as reported by Aarik *et al.* was 0.3 – 0.5 atom-%. They also obtained stoichiometric films with a 1:2 Ti:O –ratio as analysed by Auger electron spectroscopy (AES) (166). The films deposited at 100 °C by Aarik *et al.* had 1.3 – 1.6 atom-% carbon, and changing the oxygen source to H_2O_2 decreased the carbon contents to 0.6 – 1.0 atom-%. Ritala reported that most films deposited with thermal ALD from $Ti(O^iPr)_4$, $Ti(OEt)_4$, $TiCl_4$ and water were conductive enough to be measured with the standard four-point probe technique (201). The resistivities were between 1 and 100 Ωcm, and the conductivity was attributed to the tendency of titanium dioxide to form slightly oxygen deficient films when annealed in vacuum or in the presence of reducing agents.

Kim *et al.* studied the use of ozone (O_3) as the oxygen source in the deposition of titanium dioxide with $Ti(O^iPr)_4$ as the titanium precursor (167). They used a travelling-wave reactor, and obtained a saturated growth rate of 0.054 nm/cycle at 250 °C. They also reported very high dielectric constants for films deposited on ruthenium films at 250 °C. The dielectric constants were 83 and 100 on sputtered and ALD deposited ruthenium films. The dielectric constant was only 43 for a film deposited on sputtered platinum films. The films were, however, annealed in 5 % O_2/N_2 at 400 and 500 °C for 30 minutes. Results for the as deposited films were not reported. The leakage currents were approximately 0.01 $\mu A/cm^2$ up to 0.3 and 0.4 MV/cm electric fields for 27.2 nm and 25.4 nm thick films deposited on platinum and ruthenium films. The leakage currents increased rapidly with increasing electric field to 1 mA/cm^2 at 0.74 and 0.78 MV/cm for the films deposited on platinum and ruthenium films. The dielectric constants are higher and leakage currents lower than for the REALD TiO_2 films.

Lim *et al.* studied the PEALD of titanium dioxide using $Ti(O^iPr)_4$ and O_2 or an O_2-N_2 mixture at 250 °C (54). For reference, they also deposited TiO_2 using $Ti(O^iPr)_4$ and water without any additional activation. They obtained a saturated growth rate of 0.017 nm/cycle and 0.042 nm/cycle for the thermally and plasma activated processes. The reported growth rate is only half of that reported by

Ritala *et al* .(164) and a quarter of what Rahtu *et al.* reported for a higher water dose (165). Lim *et al.* obtained a higher growth rate of 0.05 nm/cycle by using a larger water dose but reported that it significantly deteriorated the film uniformity and quality. The leakage currents at 0.1 MV/cm electric field decreased four orders of magnitude as the oxygen source was changed from water to O_2-N_2 plasma, with the lowest value being approximately 1 μA/cm^2. The leakage current decreased only two orders of magnitude if O_2 plasma was used, as the oxygen source instead of water. The lowest leakage current reported by Lim *et al.* is quite similar to what was obtained with REALD. Choi *et al.* also studied the PEALD of titanium dioxide using $Ti(O^iPr)_4$ and plasma activated O_2, but no film properties or experimental details other than those related to the resistive switching properties were reported (53).

Park *et al.* studied the deposition of TiO_2 from $Ti[N(CH_3)_2]_4$ and O_2 plasma between 150 and 250 °C (55). They obtained a growth rate of 0.036 nm/cycle at 200 °C, and noted that the deposition did not proceed with molecular O_2: radicals were required. They also demonstrated conformal growth with over 95 % step coverage on approximately 1:1 aspect ratio. They reported that the films contained no carbon as analyzed by AES depth profiling, and commented that the use of plasma is most likely the reason for the low carbon content. They obtained quite low leakage currents for their post deposition annealed films, 1 μA/cm^2 at a 0.4 MV/cm electric field. However, the leakage currents were two to three orders of magnitude higher for the as-deposited films. Also Kim *et al.* studied the deposition of titanium dioxide by PEALD from $Ti[N(CH_3)_2]_4$ and O_2 plasma at 200 °C (172). They used a post-deposition laser annealing with a power density of 100 mJ/cm^2. The as-deposited films exhibited a leakage current of 0.4 mA/cm^2 at a 0.26 MV/cm electric field, and the laser annealed films showed a 3 mA/cm^2 leakage current at the same electric field. Finally, Maeng *et al.* studied the PEALD of TiO_2 from $Ti[N(CH_3)_2]_4$ and O_2 plasma at 200 °C (47). They obtained a 0.22 nm/cycle growth rate and a 0.7 mA/cm^2 leakage current at 1 MV/cm electric field. Both Park and Kim *et al.* reported much higher leakage currents than what was obtained with REALD, but Maeng

et al. demonstrated the lowest leakage currents reported so far for as-deposited ALD titanium dioxide.

Comparing the processes using titanium isopropoxide with different oxygen sources, the highest growth rate was obtained with the REALD process using oxygen radicals as the oxygen source (IV). Of the thermally activated processes, the fastest growth per cycle was obtained using H_2O_2 as the oxygen source (166). In a related study, Aarik *et al.* obtained TiO_2 with the rutile phase, and 0.18 nm/cycle growth rate at 445 °C using TiI_4 and water (163). Compared to this process, the rate of 0.195 nm/cycle obtained with the REALD process is only 10 % higher. The highest refractive index, 2.5, was obtained with the thermally activated process using titanium isopropoxide and water (164). However, even higher refractive indices, 2.4 – 2.7 and 2.8, were reported by Aarik *et al.* for crystalline, non-epitaxial and epitaxial films deposited on α-Al_2O_3 from $TiCl_4$ and water (142). An epitaxial deposition using titanium isopropoxide has not been reported. The impurity contents were not largely affected by the choice of oxygen source, as all the processes produced pure, stoichiometric films close to 250 °C. The highest dielectric constant and the lowest leakage currents were obtained by Kim *et al.* using ozone as the oxygen source, although an even lower leakage current was reported by Maeng *et al.* using $Ti[N(CH_3)_2]_4$ and O_2 plasma. Good electrical properties were obtained with the REALD films at 50 °C.

4.2.3 Tantalum oxide (V)

Tantalum oxide films were deposited with three different sequences using $Ta(OEt)_5$, oxygen radicals and water between 150 and 250 °C (Table VIII). The experiments with water were conducted at 250 °C, and the water was not activated or dissociated with the plasma discharge. With the baseline $Ta(OEt)_5$-O sequencing, saturated growth of 0.195 nm/cycle was obtained with a 0.6 second $Ta(OEt)_5$ pulse and a 3 second oxygen radical pulse (Table IX). With the overall cycle time being 8 seconds, the growth rate was 1.4 nm/min. The films grew conformally, as can be seen in the cross-sectional SEM images (Figure 10). By adding a water pulse to the $Ta(OEt)_5$-O sequencing, either before or after the

tantalum ethoxide pulse, the difference between the half reactions of $Ta(OEt)_5$-O and $Ta(OEt)_5$-H_2O can be studied.

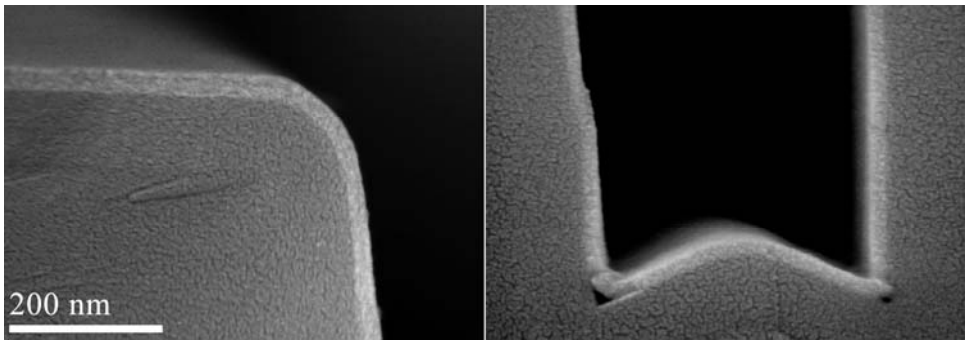

Figure 10. SEM images of a 20 nm thick Ta_2O_5 film deposited on a 4:1 aspect ratio trench. Top left part of the trench is show on the left and the bottom part on the right.

Table VIII. The precursor pulse sequences used for Ta_2O_5 deposition and the growth rates obtained with them.

Sequence / steps	1	2	3	4	5	6	Growth rate / nm/cycle
$Ta(OEt)_5$-O	$Ta(OEt)_5$	purge	O	purge			0.20
$Ta(OEt)_5$-H_2O-O	$Ta(OEt)_5$	purge	H_2O	purge	O	purge	0.11
H_2O-$Ta(OEt)_5$-O	H_2O	purge	$Ta(OEt)_5$	purge	O	purge	0.20
$Ta(OEt)_5$-H_2O	$Ta(OEt)_5$	purge	H_2O	purge			0.05

The addition of a water pulse before the tantalum precursor, according to the H_2O-$Ta(OEt)_5$-O sequence, resulted in the same growth rate as the $Ta(OEt)_5$-O deposition sequence (Table VIII). In both cases the chemisorbed tantalum ethoxide reacts with oxygen radicals. However, when the water pulse followed the tantalum ethoxide pulse, according to the $Ta(OEt)_5$-H_2O-O sequence, the growth rate decreased significantly, to 0.11 nm/cycle (Table VIII). This is still higher than what was obtained with the $Ta(OEt)_5$-H_2O sequencing, i.e. the thermally activated tantalum ethoxide-water process, 0.05 nm/cycle (Table VIII).

In both cases the chemisorbed tantalum ethoxide is reacted with water. A possible explanation for the lower growth rate of $Ta(OEt)_5$-H_2O compared to $Ta(OEt)_5$-H_2O-O is that the oxygen radical pulse in the end of the $Ta(OEt)_5$-H_2O-O sequence increases the number of adsorption sites on which tantalum ethoxide can attach to during the next reaction cycle, though not to the level obtained with the $Ta(OEt)_5$-O sequence. Thus, the amount of film grown per cycle would be closer to a complete monolayer than in the process utilizing solely water, but somewhat lower than in the process using only oxygen radicals.

The refractive index at 580 nm was 2.06 for films grown at 150 °C. Increasing the deposition temperature to 250 °C increased the refractive index to 2.21. The highest refractive index, 2.27, was obtained by the H_2O-$Ta(OEt)_5$-O pulsing sequence at 250 °C, whereas the $Ta(OEt)_5$-H_2O-O sequence resulted in a refractive index of 2.06. The film density increased with deposition temperature from 7.1 to 7.6 g/cm^3 for films deposited at 150 and 250 °C. The densities are relatively high for amorphous Ta_2O_5, as the density of crystalline Ta_2O_5 is 8.2 g/cm^3 (202). The density decreased slightly with the H_2O-$Ta(OEt)_5$-O sequencing, to 7.2 g/cm^3. Film RMS roughness was 1.4 nm for a 90 nm thick film deposited at 250°C, and increased to 2.6 nm with the H_2O-$Ta(OEt)_5$-O sequencing. Thus, the H_2O-$Ta(OEt)_5$-O sequencing produced the highest refractive index, decreased density and increased roughness.

The tantalum oxide films deposited using only oxygen radicals at 150 °C had slightly higher amount of oxygen than expected from stoichiometry (Table IX), but the film also had high amounts of carbon and hydrogen. Increasing the deposition temperature to 250 °C decreased the amount of impurities in the film and made the film more stoichiometric. The addition of a water pulse to the deposition process at 250 °C had also an effect on the film impurities: H_2O-$Ta(OEt)_5$-O sequencing improved the film purity as compared to $Ta(OEt)_5$-H_2O-O which is consistent with the refractive indices, but both still had slightly higher amount of impurities than the film deposited without the additional water pulse.

The C:H ratio in the impurities of the film deposited at 250 °C is 2:5, which suggests that the impurities may be in the form of left-over ethoxide ligands. Thus, some excess oxygen may also be in the ethoxide residues and the films deposited without the additional water pulse are more stoichiometric than the Ta:O ratio indicates. The C:H ratio is different for the films deposited with the additional water pulse, roughly 2:3. Therefore, there must be other impurities present besides ethoxide ligands, possibly left-over hydroxyl groups.

Table IX. The Ta_2O_5 film composition according to TOF-ERDA. The Ta:O ratio is calculated from the bulk composition.

Process / composition (atom-%)	Ta:O ratio	Ta	O	C	H
$Ta(OEt)_5$-O, 150 °C	2:5.6	21.6	60.7	3.3	13.8
$Ta(OEt)_5$-O, 250 °C	2:5.1	25.2	72.1	0.6	2.1
H_2O-$Ta(OEt)_5$-O, 250 °C	2:5.0	27.8	69.1	1.2	1.9
$Ta(OEt)_5$-H_2O-O, 250 °C	2:5.2	26.8	68.5	1.9	2.8
Stoichiometric Ta_2O_5	2:5	28.6	71.4	0	0

Overall, the dielectric constant increased with the deposition temperature. The dielectric constants were 28 and 36 for films deposited on platinum at 150 and 250 °C. The leakage current density at 1 MV/cm electric field was 0.01 μA/cm^2 for films grown both at 150 and 250 °C. The leakage current measurements were probably limited by the simple measuring setup and the actual values may be even lower. The leakage currents of 1 μA/cm^2 were obtained with 2.3 and 1.6 MV/cm applied electric fields for films deposited at 150 and 250 °C, and the catastrophic breakdown occurred at 4.1 and 3.1 MV/cm. The leakage currents increased in a linear fashion up to the catastrophic breakdown. Adding water to the pulsing sequence at 250 °C decreased the dielectric constant and increased the leakage currents for both the H_2O-$Ta(OEt)_5$-O and $Ta(OEt)_5$-H_2O-O sequencings. The deterioration was however minor with the $Ta(OEt)_5$-H_2O-O sequencing, but quite severe with the H_2O-$Ta(OEt)_5$-O sequencing. This is

surprising as the H_2O-$Ta(OEt)_5$-O film has lower impurity contents and is closer to stoichiometric than the film deposited with the $Ta(OEt)_5$-H_2O-O sequence. The leakage current densities at 1 MV/cm were 0.45 mA/cm^2 and 5 μA/cm^2, and the dielectric constants 31 and 34 for the H_2O-$Ta(OEt)_5$-O and $Ta(OEt)_5$-H_2O-O sequencing. This suggests that the poor electrical results are related to the H_2O-$Ta(OEt)_5$ half-reaction where tantalum ethoxide adsorbs on a hydroxyl-covered surface. On the other hand, the slow growth seems to be connected to the $Ta(OEt)_5$-H_2O half-reaction where adsorbed tantalum ethoxide reacts with water.

Kukli *et al.* deposited tantalum oxide with thermally activated ALD using $Ta(OEt)_5$ and water between 150 and 450 °C (181). From 250 to 325 °C deposition temperatures, the growth rate was 0.04 nm/cycle, and decreased both above and below this temperature range. The refractive index increased from 1.9 to 2.23 when the deposition temperature was increased from 150 to 300 °C, and remained at the higher value up to 450 °C. The refractive index at 150 °C deposition temperature was slightly lower than with the REALD process, but increased to an almost identical value at higher temperatures. The films deposited at 250 and 325 °C contained 4 and 0.6 atom-% of hydrogen as analysed by nuclear reaction analysis (NRA). This is slightly higher than what was obtained with the REALD process, but interestingly very similar to what was obtained with the Ta-H_2O-O sequencing (Table IX). The films deposited at both temperatures were very close to being stoichiometric Ta_2O_5. Dielectric constants of 21 and 25 and leakage currents of 4.0 and 2.3 mA/cm^2 were obtained for films deposited at 250 and 325 °C. Both the dielectric constant and the leakage current behaviour were improved with the REALD process.

Tantalum oxide has been deposited with PEALD by Song *et al.* at 260 °C using $Ta(OEt)_5$ and oxygen plasma (46). The growth rate was 0.075 nm/cycle, which is slightly higher than with using water as the oxygen source, but much slower than with the REALD process. The film composition was analyzed by TOF-ERDA, and the films were found to be stoichiometric both before and after the post deposition annealing, and contained less than 0.1 atom-% of carbon and hydrogen. They obtained leakage currents of 10 and 1 μA/cm^2 at 1 MV/cm

electric field for the as-deposited and oxygen annealed films. These are higher values than what was obtained with the REALD and photoassisted ALD (Photo-ALD) processes (see below). They however obtained a quite high dielectric constant of 38, which is higher than that obtained with the REALD process.

Photoassisted ALD has been used to deposit tantalum oxide from $Ta(OEt)_5$ and water between 170 and 400 °C (186) by Kwak *et al.*, and from $Ta(OEt)_5$ and O_2 between 170 and 350 °C by Lee *et al.* (187). They both used a UV lamp with 185 nm radiation to provide additional energy to the reactions. Using water as the oxygen source, a 0.042 nm/cycle growth rate was obtained without the photoassistance and 0.047 nm/cycle with Photo-ALD. Using photoactivated oxygen as the oxygen source, the growth rate was even lower, only 0.037 nm/cycle. The growth rate without the additional energy is in good accordance to the values reported by Kukli *et al.* (181). Although the growth rate did not increase significantly, Kwak *et al.* found that the cycle times could be reduced with the Photo-ALD, and thus the throughput was increased (186). The refractive indices were between 2.12 and 2.16 for films deposited with Photo-ALD between 190 and 300 °C. The film grown at 260 °C also had a quite typical dielectric constant of 23. A significant improvement was however obtained in the leakage current, which decreased from the 4 mA/cm^2 reported by Kukli *et al.* (181) to 0.6 – 1.0 $\mu A/cm^2$ at an 1 MV/cm applied electric field for a film deposited at 260 °C. Lee *et al.* also obtained remarkably low leakage currents, only 0.01 $\mu A/cm^2$ at the same, 1 MV/cm applied field for films deposited at 350 °C (187). The dielectric constant of those films was 22 – 25. The leakage currents obtained by Lee *et al.* are of the same magnitude as obtained with the REALD process at 250 °C, only with a slightly lower dielectric constant. The authors speculated that the low leakage currents are a result of highly reactive oxygen atom species generated by the UV radiation. The film growth is, however, much slower than with either PEALD or REALD, though it is closer to the PEALD than REALD growth rate.

Finally, very good electrical results have been obtained by Hausmann *et al.* with a thermally activated process utilizing pentakis(dimethylamido)tantalum(V),

$Ta[N(CH_3)_2]_5$ or tris(diethylamido)(ethylimido)tantalum(V), $Ta[(NEt)(NEt_2)]_3$, and water at deposition temperatures ranging from 50 to 350 °C (183). They obtained a 0.065 nm/cycle growth rate with both tantalum precursors, which is slower than with REALD but slightly higher than for the thermally activated process using $Ta(OEt)_5$ and water. They obtained also good conformality, 6.6 g/cm^3 density, and a refractive index of 2.1 for the films deposited between 50 and 350 °C. The deposition at 50 °C, however, required very long cycle times: 300 s purge periods were used to allow sufficient purging of the precursors. The films had a dielectric constant of 28, and the catastrophic breakdown occurred at a 4.5 MV/cm electric field. The leakage currents were below 1 μA/cm^2 for a 1.5 MV/cm electric field, which are quite similar to the values obtained with the PEALD process by Song *et al.*

Of the previously discussed processes using tantalum ethoxide and different oxygen sources, the REALD process produced the highest growth rate and film density. The films deposited with REALD also exhibited a high dielectric constant and low leakage current, very similarly to the PEALD processes. The highest refractive index was obtained with the thermally activated tantalum ethoxide-water process and the highest film purity with the PEALD process by Song *et al.*

4.2.4 Other experiments

Table X presents processes to deposit oxides which were tried but not studied further or published.

Table X. Experimental parameters for less studied or unsuccessful oxide deposition experiments

Material / substrate	Metal precursor	Reactive gas	Temperature / °C	Result
CuO / Si, glass	$Cu(thd)_2$, $Cu(acac)_2$	O_2	150 - 250	Growth on glass and Si
$SrTiO_3$ / Si,	$SrCp_2$,	O_2	275	Growth on all

glass, Pt	$Ti(O^iPr)_4$			substrates, single experiment
SiO_2 / Si, glass	TEOS	O_2	25 – 300	No growth
ZnO / Si, glass	$Zn(CH_3)_2$	O_2	150 – 250	Growth on Si and glass
Nb_2O_5 / Si, glass	$Nb(OEt)_5$	O_2	250	Growth on Si and glass, single experiment
Cr_2O_3 / Si, glass	$Cr(acac)_3$	O_2	150 - 250	Growth on Si and glass, non-uniform growth
RuO_2 / glass	$RuCp_2$	O_2	100 – 300	Metallic Ru at over 200 °C, possibly RuO_2 at 100 °C
NiO / Si, glass	$Ni(O^iPrN(CH_3)_2)_2$	O_2	100	No growth

The deposition of chromium oxide resulted in non-uniform growth. As the deposition area is circular, two concentric areas were obtained in this case: the centre area had very little film growth and the surrounding areas had a thicker film. This may be a result of precursor desorption, possibly by a formation of some volatile species, or etching. The deposition using $RuCp_2$ and oxygen radicals resulted in metallic ruthenium films at 200 °C as the precursor reacted with molecular oxygen. The deposition with molecular oxygen should not, however, proceed at such a low temperature. The deposition at 100 °C resulted in a film which had a lower density and higher resistivity than metallic ruthenium. Both density and resistivity were, however, in accordance with the properties of ruthenium oxide.

5. CONCLUSION

The increasing interest towards ALD in general raises hope that techniques now under basic research could become more common in the future. One such technique is the use of plasmas and radicals in the deposition of thin films by ALD. Radical Enhanced ALD offers several benefits over conventional, thermally activated ALD processes: possibility to deposit at very low temperatures, increased growth rate and the ability to use a widely applicable reducing agent, hydrogen radicals.

The deposition of copper and silver with REALD can be considered successful. Both processes were unproblematic, and both copper and silver grew conformally in the ALD mode. The material purity was also good in both cases, and the film properties were also very promising. The successful deposition of silver, in particular, is very encouraging as it is a novel material for ALD. On the basis of the REALD copper and silver, it seems that hydrogen radicals are good reducing agents. On the other hand, higher fluxes may be needed for the reduction metals at higher oxidation states than copper or silver.

The deposition of oxides with REALD was also successful. A common feature in the REALD of oxides was their high growth rate, as compared to their thermally activated counterparts. The high growth rates may be a result of the oxygen radicals forming volatile reaction by-products more efficiently. Therefore, the growth surface would be cleaner, and have a higher number of free adsorption sites for the metal precursor. Thus, a higher growth rate would be obtained. The chemical nature of the adsorption sites is not known, however.

Comparing the deposition of aluminium, tantalum, and titanium oxides to their thermal ALD counterparts, the most improvement in the film properties was obtained in the case of aluminium oxide, where the metal precursor was a metal alkyl. Less improvement was obtained in the case of titanium and tantalum oxides, where the metal precursors were alkoxides. This raises a

question whether the oxygen radicals are better suited for use with metal alkyls than with alkoxides. More generally, are some precursors more suitable to be used with oxygen radicals while others produce better results with water? And finally, is there an ideal group of metal precursors which react optimally with oxygen radicals? Similar questions apply naturally to the processes utilizing hydrogen radicals, both requiring systematic research.

A major advantage of REALD is that the lowest deposition temperature is governed only by the condensation of metal precursor, as the non-metal reactant is so highly reactive. On the other hand, a possibility for contamination and slow deposition still exists at low deposition temperatures if poorly volatile or bulky reaction by-products are formed. If the radicals react also with the by-products, their volatility may be improved.

The high reactivity of radicals and thus recombination excludes the use of REALD in highly porous materials and where penetration is required. Batch processing is also very challenging with REALD, as is deposition on large areas. With proper reactor design and a large area plasma source, these may become possible. Decreasing the reactor pressure will decrease recombination but makes pumping slower. Equipment-wise the greatest weakness of REALD at the moment is the poor availability, and thus the heterogeneity of the deposition equipment. The currently used REALD reactor has long cycle times as compared to similar ALD reactors operating without a plasma source. The long cycle times arise mainly from the operation of the plasma discharge. This is somewhat alleviated by the high growth rates and thus the high throughput obtained with silver and oxide processes. Despite the limitations of the reactor, the successful deposition of metals and oxides by REALD shows a lot of promise, warrants further study of REALD processes, and hopefully will encourage further development of commercial deposition equipment.

6. REFERENCES

(1) M. Ritala and M. Leskelä in *Handbook of Thin Films Materials,* edited by Nalwa, Academic Press, 2002, San Diego, CA, U.S.A., p. 103

(2) T. M. Mayer, J. W. Elam, S. M. George, P. G. Kotula and R. S. Goeke, *Appl. Phys. Lett.,* 82 (2003) 2883

(3) J. L. Cecchi in *Handbook of plasma processing technology,* edited by Rossnagel, Cuomo and Westwood, Noyes, 1990, Park Ridge, New Jersey, U.S.A., p. 14

(4) N. S. J. Braithwaite, *Plasma Sources Sci. Technol.,* 9 (2000) 517

(5) R. Reif in *Handbook of plasma processing technology,* edited by Rossnagel, Cuomo and Westwood, Noyes, 1990, Park Ridge, New Jersey, U.S.A., p. 261

(6) H. Conrads and M. Schmidt, *Plasma Sources Sci. Technol.,* 9 (2000) 441

(7) Y. J. Lee and S. Kang, *Thin Solid Films,* 446 (2004) 227

(8) Y. J. Lee, *J. Cryst. Growth,* 266 (2004) 568

(9) J. Y. Kim, D. Y. Kim, H. O. Park and H. Jeon, *J. Electrochem. Soc.,* 152 (2005) G29

(10) G. Lucovsky, D. V. Tsu and R. J. Markunas in *Handbook of plasma processing technology,* edited by Rossnagel, Cuomo and Westwood, Noyes, 1990, Park Ridge, New Jersey, U.S.A., p. 387

(11) D. B. Fraser and W. D. Westwood in *Handbook of plasma processing technology,* edited by Rossnagel, Cuomo and Westwood, Noyes, 1990, Park Ridge, New Jersey, U.S.A., p. 2

(12) J. S. Logan in *Handbook of plasma processing technology,* edited by Rossnagel, Cuomo and Westwood, Noyes, 1990, Park Ridge, New Jersey, U.S.A., p. 140-159

(13) G. S. Oehrlein in *Handbook of plasma processing technology,* edited by Rossnagel, Cuomo and Westwood, Noyes, 1990, Park Ridge, New Jersey, U.S.A., p. 198-232

(14) G. Oya, M. Yoshida and Y. Sawada, *Appl. Phys. Lett.,* 51 (1987) 1143

(15) R. L. Puurunen, *J. Appl. Phys.,* 97 (2005) 121301

(16) M. Putkonen and L. Niinistö, *Thin Solid Films,* 514 (2006) 145

(17) M. D. Groner, F. H. Fabreguette, J. W. Elam and S. M. George, *Chem. Mater.,* 16 (2004) 639

(18) R. Messier, J. E. Yehoda and L. J. Pilione in *Handbook of plasma processing technology,* edited by Rossnagel, Cuomo and Westwood, Noyes, 1990, Park Ridge, New Jersey, U.S.A., p. 448

(19) Y. J. Lee and S. Kang, *Electrochem. Solid-State Lett.,* 5 (2002) C91

(20) C. Jeong, J. Lee and S. Joo, *Jpn. J. Appl. Phys. Part 1,* 40 (2001) 285

(21) S. Ha, E. Choi, S. Kim and J. Sung Roh, *Thin Solid Films,* 476 (2005) 252

(22) B. Hoex, S. B. S. Heil, E. Langereis, M. C. M. van de Sanden and Kessels, W. M. M., *Appl. Phys. Lett.,* 89 (2006) 042112

(23) B. H. Kim, W. S. Jeon, S. H. Jung and B. T. Ahn, *Electrochem. Solid-State Lett.,* 8 (2005) G294

(24) J. W. Lim and S. J. Yun, *Electrochem. Solid-State Lett.,* 7 (2004) F45

(25) J. W. Lim, S. J. Yun, Y. H. Kim, C. Y. Sohn and J. Lee, *Electrochem. Solid-State Lett.,* 7 (2004) G185

(26) S. J. Yun, J. W. Lim and J. Lee, *Electrochem. Solid-State Lett.,* 7 (2004) C13

(27) S. J. Yun, Y. Ko and J. W. Lim, *Appl. Phys. Lett.,* 85 (2004) 4896

(28) J. W. Lim, S. J. Yun and J. Lee, *Electrochem. Solid-State Lett.,* 8 (2005) F25

(29) J. W. Lim, S. J. Yun and J. Lee, *Electrochem. Solid-State Lett.,* 9 (2006) F8

(30) H. Lee and H. Kim, *Electrochem. Solid-State Lett.,* 9 (2006) G323

(31) C. Jezewski, W. A. Lanford, C. J. Wiegand, J. P. Singh, P. Wang, J. J. Senkevich and T. Lu, *J. Electrochem. Soc.,* 152 (2005) C60

(32) F. K. Shan, G. X. Liu, W. J. Lee, G. H. Lee, I. S. Kim and B. C. Shin, *J. Appl. Phys.,* 98 (2005) 023504

(33) K. Endo and T. Tatsumi, *Jpn. J. Appl. Phys. Part 2,* 42 (2003) L685

(34) J. Kim, S. Kim, H. Jeon, M. -. Cho, K. -. Chung and C. Bae, *Appl. Phys. Lett.,* 87 (2005) 053108

(35) J. Kim, S. Kim, H. Kang, J. Choi, H. Jeon, M. Cho, K. Chung, S. Back, K. Yoo and C. Bae, *J. Appl. Phys.,* 98 (2005) 094504

(36) Y. Lee, S. Kim, J. Koo, I. Kim, J. Choi, H. Jeon and Y. Won, *J. Electrochem. Soc.,* 153 (2006) G353

(37) J. Chae, H. Park and S. Kang, *Electrochem. Solid-State Lett.,* 5 (2002) C64

(38) O. Kwon, S. Kwon, H. Park and S. Kang, *Electrochem. Solid-State Lett.,* 7 (2004) C46

(39) O. Kwon, S. Kwon, H. Park and S. Kang, *J. Electrochem. Soc.,* 151 (2004) C753

(40) S. Kwon, O. Kwon, J. Min and S. Kang, *J. Electrochem. Soc.,* 153 (2006) G578

(41) J. H. Lee, Y. J. Cho, Y. S. Min, D. Kim and S. W. Rhee, *J. Vac. Sci. Technol. A,* 20 (2002) 1828

(42) W. Lee, I. You, S. Ryu, B. Yu, K. Cho, S. Yoon and C. Lee, *Jpn. J. Appl. Phys. Part 1,* 40 (2001) 6941

(43) J. Park, M. Lee, C. Lee and S. Kang, *Electrochem. Solid-State Lett.,* 4 (2001) C17

(44) J. Park, H. Park and S. Kang, *J. Electrochem. Soc.,* 149 (2002) C28

(45) A. Furuya, H. Tsuda and S. Ogawa, *J. Vac. Sci. Technol. B,* 23 (2005) 979

(46) H. Song, C. Lee and S. Kang, *Electrochem. Solid-State Lett.,* 4 (2001) F13

(47) W. J. Maeng and H. Kim, *Electrochem. Solid-State Lett.,* 9 (2006) G191

(48) Y. J. Lee and S. Kang, *Electrochem. Solid-State Lett.,* 6 (2003) C70

(49) Y. J. Lee and S. Kang, *Appl. Phys. Lett.,* 86 (2005) 071919

(50) D. Kim, Y. J. Kim, J. Park and J. H. Kim, *Materials Science and Engineering: C,* 24 (2004) 289

(51) K. Elers, J. Winkler, K. Weeks and S. Marcus, *J. Electrochem. Soc.,* 152 (2005) G589

(52) E. Langereis, S. B. S. Heil, M. C. M. van de Sanden and Kessels, W. M. M., *J. Appl. Phys.,* 100 (2006) 023534

(53) B. J. Choi, S. Choi, K. M. Kim, Y. C. Shin, C. S. Hwang, S. Hwang, S. Cho, S. Park and S. Hong, *Appl. Phys. Lett.,* 89 (2006) 012906

(54) J. W. Lim, S. J. Yun and J. Lee, *Electrochem. Solid-State Lett.,* 7 (2004) F73

(55) J. Park, W. Lee, G. Lee, I. Kim, B. Shin and S. Yoon, *Integrated Ferroelectr.,* 68 (2004) 129

(56) J. Park and S. Kang, *Electrochem. Solid-State Lett.,* 7 (2004) C87

(57) D. Kim, Y. J. Kim, Y. S. Song, B. Lee, J. H. Kim, S. Suh and R. G. Gordon, *J. Electrochem. Soc.,* 150 (2003) C740

(58) Y. Kim, J. Koo, J. Han, S. Choi, H. Jeon and C. Park, *J. Appl. Phys.,* 92 (2002) 5443

(59) S. J. Yun, J. W. Lim and J. Lee, *Electrochem. Solid-State Lett.,* 7 (2004) F81

(60) S. J. Yun, J. W. Lim and J. Lee, *Electrochem. Solid-State Lett.,* 8 (2005) F47

(61) M. Cho, H. B. Park, J. Park, S. W. Lee, C. S. Hwang, J. Jeong, H. S. Kang and Y. W. Kim, *J. Electrochem. Soc.,* 152 (2005) F49

(62) S. Kim, J. Kim, J. Choi, H. Kang, H. Jeon, W. Cho, K. An, T. Chung, Y. Kim and C. Bae, *Electrochem. Solid-State Lett.,* 9 (2006) G200

(63) T. T. Van and J. P. Chang, *Appl. Surf. Sci.,* 246 (2005) 250

(64) H. Kang, S. Kim, J. Choi, J. Kim, H. Jeon and C. Bae, *Electrochem. Solid-State Lett.,* 9 (2006) G211

(65) S. Sugahara, M. Kadoshima, T. Kitamura, S. Imai and M. Matsumura, *Appl. Surf. Sci.,* 90 (1995) 349

(66) S. Sugahara, K. Hosaka and M. Matsumura, *Appl. Surf. Sci.,* 130-132 (1998) 327

(67) G. A. T. Eyck, J. J. Senkevich, F. Tang, D. Liu, S. Pimanpang, T. Karaback, G. Wang, T. Lu, C. Jezewski and W. A. Lanford, *Chem. Vap. Deposition,* 11 (2005) 60

(68) D. Kil, J. Lee and J. Roh, *Chem. Vap. Deposition,* 8 (2002) 195

(69) S. W. Lee, O. S. Kwon and C. S. Hwang, *Microelectron. Eng.,* 80 (2005) 158

(70) S. M. Rossnagel, A. Sherman and F. Turner, *J. Vac. Sci. Technol. B,* 18 (2000) 2016

(71) H. Kim, C. J. Cabral, C. Lavoie and S. M. Rossnagel, *J. Vac. Sci. Technol. B,* 20 (2002) 1321

(72) H. Kim and S. M. Rossnagel, *Thin Solid Films,* 441 (2003) 311

(73) H. Kim, A. J. Kellock and S. M. Rossnagel, *J. Appl. Phys.,* 92 (2002) 7080

(74) H. Kim, C. Lavoie, M. Copel, V. Narayanan, D. -. Park and S. M. Rossnagel, *J. Appl. Phys.,* 95 (2004) 5848

(75) H. Kim, C. Detavenier, O. van der Straten, S. M. Rossnagel, A. J. Kellock and D. -. Park, *J. Appl. Phys.,* 98 (2005) 014308

(76) H. Kim and S. M. Rossnagel, *J. Vac. Sci. Technol. A,* 20 (2002) 802

(77) S. B. S. Heil, E. Langereis, A. Kemmeren, F. Roozeboom, M. C. M. van de Sanden and Kessels, W. M. M., *J. Vac. Sci. Technol. A,* 23 (2005) L5

(78) F. Greer, D. Fraser, J. W. Coburn and D. B. Graves, *J. Vac. Sci. Technol. A,* 21 (2003) 96

(79) J. Y. Kim, Y. Kim and H. Jeon, *Jpn. J. Appl. Phys. Part 2,* 42 (2003) L414

(80) J. Y. Kim, S. Seo, D. Y. Kim, H. Jeon and Y. Kim, *J. Vac. Sci. Technol. A,* 22 (2004) 8

(81) T. T. Van and J. P. Chang, *Surf. Sci.,* 596 (2005) 1

(82) J. Y. Kim, S. H. Kim, H. Seo, J. Kim and H. Jeon, *Electrochem. Solid-State Lett.,* 8 (2005) G82

(83) B. S. Lim, A. Rahtu and R. G. Gordon, *Nature Mater.,* 2 (2003) 749

(84) M. Utriainen, M. Kroger-Laukkanen, L. Johansson and L. Niinistö, *Appl. Surf. Sci.,* 157 (2000) 151

(85) M. Juppo, M. Ritala and M. Leskelä, *J. Vac. Sci. Technol. A,* 15 (1997) 2330

(86) P. Mårtensson and J. Carlsson, *Chem. Vap. Deposition,* 3 (1997) 45

(87) P. Mårtensson and J. Carlsson, *J. Electrochem. Soc.,* 145 (1998) 2926

(88) R. Solanki and B. Pathangey, *Electrochem. Solid-State Lett.,* 3 (2000) 479

(89) J. Huo, R. Solanki and J. McAndrew, *J. Mater. Res.,* 17 (2002) 2394

(90) T. Törndahl, M. Ottosson and J. Carlsson, *Thin Solid Films,* 458 (2004) 129

(91) M. Juppo, M. Vehkamäki, M. Ritala and M. Leskelä, *J. Vac. Sci. Technol. A,* 16 (1998) 2845

(92) T. Aaltonen, P. Alén, M. Ritala and M. Leskelä, *Chem. Vap. Deposition,* 9 (2003) 45

(93) T. Aaltonen, A. Rahtu, M. Ritala and M. Leskelä, *Electrochem. Solid-State Lett.,* 6 (2003) C130

(94) M. Lashdaf, T. Hatanpää, A. O. I. Krause, J. Lahtinen, M. Lindblad and M. Tiitta, *Appl. Catal. A,* 241 (2003) 51

(95) T. Aaltonen, M. Ritala, K. Arstila, J. Keinonen and M. Leskelä, *Chem. Vap. Deposition,* 10 (2004) 215

(96) O. Kwon, J. Kim, H. Park and S. Kang, *J. Electrochem. Soc.,* 151 (2004) G109

(97) T. Aaltonen, M. Ritala and M. Leskelä, *Electrochem. Solid-State Lett.,* 8 (2005) C99

(98) A. M. Molenbroek, S. Haukka and B. S. Clausen, *J. Phys. Chem. B,* 102 (1998) 10680

(99) J. J. Senkevich, F. Tang, D. Rogers, J. T. Drotar, C. Jezewski, W. A. Lanford, G. -. Wang and T. -. Lu, *Chem. Vap. Deposition,* 9 (2003) 258

(100) G. A. T. Eyck, S. Pimanpang, H. Bakhru, T. -. Lu and G. -. Wang, *Chem. Vap. Deposition,* 12 (2006) 290

(101) J. W. Klaus, S. J. Ferro and S. M. George, *Appl. Surf. Sci.,* 162-163 (2000) 479

(102) J. W. Klaus, S. J. Ferro and S. M. George, *Thin Solid Films,* 360 (2000) 145

(103) J. W. Elam, C. E. Nelson, R. K. Grubbs and S. M. George, *Thin Solid Films,* 386 (2001) 41

(104) J. W. Elam, C. E. Nelson, R. K. Grubbs and S. M. George, *Surf. Sci.,* 479 (2001) 121

(105) T. Aaltonen, M. Ritala, V. Sammelselg and M. Leskelä, *J. Electrochem. Soc.,* 151 (2004) G489

(106) T. Aaltonen, M. Ritala, T. Sajavaara, J. Keinonen and M. Leskelä, *Chem. Mater.,* 15 (2003) 1924

(107) M. Ritala, M. Leskelä, E. Rauhala and P. Haussalo, *J. Electrochem. Soc.,* 142 (1995) 2731

(108) M. Ritala, T. Asikainen, M. Leskelä, J. Jokinen, R. Lappalainen, M. Utriainen, L. Niinistö and E. Ristolainen, *Appl. Surf. Sci.,* 120 (1997) 199

(109) R. Rosenberg, D. C. Edelstein, C. -. Hu and K. P. Rodbell, *Annu. Rev. Mater. Sci.,* 30 (2000) 220

(110) S. Chiu, J. Shieh, S. Chang, K. Lin, B. Dai, C. Chen and M. Feng, *J. Vac. Sci. Technol. B,* 18 (2000) 2835

(111) T. Törndahl, J. Lu, M. Ottosson and J. Carlsson, *J. Cryst. Growth,* 276 (2005) 102

(112) S. Haukka, N. Raaijmakers, K. -. Elers, J. Kostamo, W. Li, H. Sprey, P. J. Soininen and M. Tuominen, *Interconnect Technology Conference, 2002.Proceedings of the IEEE 2002 International,* 2002

(113) R. Manepalli, F. Stepniak, S. A. Bidstrup-Allen and P. A. Kohl, *IEEE Trans. Adv. Pack.,* 22 (1999) 4

(114) M. Hauder, J. Gstottner, W. Hansch and D. Schmitt-Landsiedel, *Appl. Phys. Lett.,* 78 (2001) 838

(115) L. Gao, J. Gstottner, R. Emling, M. Balden, C. Linsmeier, A. Wiltner, W. Hansch and D. Schmitt-Landsiedel, *Microelectron. Eng.,* 76 (2004) 76

(116) L. Gao, P. Harter, C. Linsmeier, J. Gstottner, R. Emling and D. Schmitt-Landsiedel, *Materials Science in Semiconductor Processing,* 7 (2004) 331

(117) L. Gao, P. Harter, C. Linsmeier, A. Wiltner, R. Emling and D. Schmitt-Landsiedel, *Microelectron. Eng.,* 82 (2005) 296

(118) M. Boccas, T. Vucina, C. Araya, E. Vera and C. Ahhee, *Thin Solid Films,* 502 (2006) 275

(119) M. A. Butler and A. J. Ricco, *Appl. Phys. Lett.,* 53 (1988) 1471

(120) A. J. Nagy, G. Mestl and R. Schlogl, *J. Catal.,* 188 (1999) 58

(121) A. Andreasen, H. Lynggaard, C. Stegelmann and P. Stoltze, *Surf. Sci.,* 544 (2003) 5

(122) A. Ayame, S. Eimaeda, L. Feng and H. Hayasaka, *Appl. Catal. A,* 304 (2006) 93

(123) D. X. Yang, B. Shashishekar, H. D. Chopra, P. J. Chen and Egelhoff, W. F. Jr, *J. Appl. Phys.,* 2001

(124) H. D. Chopra, D. X. Yang, P. J. Chen and Egelhoff, W. F. Jr, *Phys. Rev. B: Condens. Matter,* 65 (2002) 094433/1

(125) K. Chi and Y. Lu, *Chem. Vap. Deposition,* 7 (2001) 117

(126) L. Zanotto, F. Benetollo, M. Natali, G. Rossetto, P. Zanella, S. Kaciulis and A. Mezzi, *Chem. Vap. Deposition,* 10 (2004) 207

(127) M. Ritala, H. Saloniemi, M. Leskelä, T. Prohaska, G. Friedbacher and M. Grasserbauer, *Thin Solid Films,* 286 (1996) 54

(128) D. Riihelä, M. Ritala, R. Matero and M. Leskelä, *Thin Solid Films,* 289 (1996) 250

(129) K. Kukli, J. Ihanus, M. Ritala and M. Leskelä, *J. Electrochem. Soc.,* 144 (1997) 300

(130) A. C. Dillon, A. W. Ott, J. D. Way and S. M. George, *Surf. Sci.,* 322 (1995) 230

(131) Y. Kim, S. M. Lee, C. S. Park, S. I. Lee and M. Y. Lee, *Appl. Phys. Lett.,* 71 (1997) 3604

(132) R. Matero, A. Rahtu, M. Ritala, M. Leskelä and T. Sajavaara, *Thin Solid Films,* 368 (2000) 1

(133) M. D. Groner, J. W. Elam, F. H. Fabreguette and S. M. George, *Thin Solid Films,* 413 (2002) 186

(134) J. B. Kim, D. R. Kwon, K. Chakrabarti, C. Lee, K. Y. Oh and J. H. Lee, *J. Appl. Phys.,* 92 (2002) 6739

(135) J. Kim, K. Chakrabarti, J. Lee, K. Oh and C. Lee, *Mater. Chem. Phys.,* 78 (2003) 733

(136) R. Kuse, M. Kundu, T. Yasuda, N. Miyata and A. Toriumi, *J. Appl. Phys.,* 94 (2003) 6411

(137) L. Hiltunen, H. Kattelus, M. Leskelä, M. Makela, L. Niinistö, E. Nykänen, P. Soininen and M. Tiitta, *Mater. Chem. Phys.,* 28 (1991) 379

(138) W. Cho, K. Sung, K. An, S. S. Lee, T. Chung and Y. Kim, *Papers from the 49th International Symposium of the American Vacuum Society,* 2003

(139) K. Kukli, M. Ritala, M. Leskelä and J. Jokinen, *J. Vac. Sci. Technol. A,* 15 (1997) 2214

(140) M. Ritala, K. Kukli, A. Rahtu, P. I. Räisänen, M. Leskelä, T. Sajavaara and J. Keinonen, *Science,* 288 (2000) 319

(141) J. M. Bennett, E. Pelletier, G. Albrand, J. Borgogno, B. Lazarides, C. Carniglia, R. Schmell, T. Allen, T. Tuttle-Hart, K. Guenther and A. Saxer, *Appl. Opt.,* 28 (1989) 3303

(142) J. Aarik, A. Aidla, H. Mändar, T. Uustare, M. Schuisky and A. Hårsta, *J. Cryst. Growth,* 242 (2002) 189

(143) G. D. Wilk, R. M. Wallace and J. M. Anthony, *J. Appl. Phys.,* 89 (2001) 5243

(144) J. Wu, S. Hayakawa, K. Tsuru and A. Osaka, *Thin Solid Films,* 414 (2002) 275

(145) V. Pore, A. Rahtu, M. Leskelä, M. Ritala, T. Sajavaara and J. Keinonen, *Chem. Vap. Deposition,* 10 (2004) 143

(146) M. Anpo, S. Dohshi, M. Kitano, Y. Hu, M. Takeuchi and M. Matsuoka, *Annu. Rev. Mater. Res.,* 35 (2005) 1

(147) M. Ritala, M. Leskelä, E. Nykänen, P. Soininen and L. Niinistö, *Thin Solid Films,* 225 (1993) 288

(148) M. Ritala, M. Leskelä, L. Johansson and L. Niinistö, *Thin Solid Films,* 228 (1993) 32

(149) S. Haukka, E. Lakomaa, O. Jylhä, J. Vilhunen and S. Hornytzkyj, *Langmuir,* 9 (1993) 3497

(150) S. Haukka, E. Lakomaa and A. Root, *J. Phys. Chem.,* 97 (1993) 5085

(151) J. Aarik, A. Aidla, T. Uustare and V. Sammelselg, *J. Cryst. Growth,* 148 (1995) 268

(152) J. Aarik, A. Aidla, T. Uustare, A. Kiisler and V. Sammelselg, *Thin Solid Films,* 305 (1997) 270

(153) R. Matero, A. Rahtu and M. Ritala, *Chem. Mater.,* 13 (2001) 4506

(154) B. J. Ninness, D. W. Bousfield and C. P. Tripp, *Colloids Surf., A,* 214 (2003) 195

(155) J. D. Ferguson, A. R. Yoder, A. W. Weimer and S. M. George, *Appl. Surf. Sci.,* 226 (2004) 393

(156) M. S. Sander, M. J. Côté, W. Gu, B. M. Kile and C. P. Tripp, *Adv. Mater.,* 16 (2004) 2052

(157) W. Gu and C. P. Tripp, *Langmuir,* 21 (2005) 211

(158) J. S. King, E. Graugnard and C. J. Summers, *Adv. Mater.,* 17 (2005) 1010

(159) K. Kukli, M. Ritala, M. Schuisky, M. Leskelä, T. Sajavaara, J. Keinonen, T. Uustare and A. Hårsta, *Chem. Vap. Deposition,* 6 (2000) 303

(160) M. Schuisky, A. Hårsta, A. Aidla, K. Kukli, A. Kiisler and J. Aarik, *J. Electrochem. Soc.,* 147 (2000) 3319

(161) M. Schuisky, J. Aarik, K. Kukli, A. Aidla and A. Hårsta, *Langmuir,* 17 (2001) 5508

(162) M. Schuisky, K. Kukli, J. Aarik, J. Lu and A. Hårsta, *J. Cryst. Growth,* 235 (2002) 293

(163) J. Aarik, A. Aidla, T. Uustare, K. Kukli, V. Sammelselg, M. Ritala and M. Leskelä, *Appl. Surf. Sci.,* 193 (2002) 277

(164) M. Ritala, M. Leskelä, L. Niinistö and P. Haussalo, *Chem. Mater.,* 5 (1993) 1174

(165) A. Rahtu and M. Ritala, *Chem. Vap. Deposition,* 8 (2002) 21

(166) J. Aarik, A. Aidla, T. Uustare, M. Ritala and M. Leskelä, *Appl. Surf. Sci.,* 161 (2000) 385

(167) S. K. Kim, W. Kim, K. Kim, C. S. Hwang and J. Jeong, *Appl. Phys. Lett.,* 85 (2004) 4112

(168) M. Ritala, M. Leskelä and E. Rauhala, *Chem. Mater.,* 6 (1994) 556

(169) A. Rahtu, K. Kukli and M. Ritala, *Chem. Mater.,* 13 (2001) 817

(170) J. Aarik, J. Karlis, H. Mändar, T. Uustare and V. Sammelselg, *Appl. Surf. Sci.,* 181 (2001) 339

(171) I. Kim, H. L. Tuller, H. Kim and J. Park, *Appl. Phys. Lett.,* 85 (2004) 4705

(172) J. Kim, W. Lee, J. Kim and S. Yoon, *Metals and Materials International,* 11 (2005) 285

(173) C. Chaneliere, J. L. Autran, B. Balland and R. A. B. Devine, *Materials Science and Engineering: R: Reports,* 22 (1998) 269

(174) D. Yoon, J. Roh, H. K. Baik and S. Lee, *Critical Reviews in Solid State and Materials Sciences,* 27 (2002) 143

(175) K. Ahn, Y. Nah, Y. Sung, K. Cho, S. Shin and J. Park, *Appl. Phys. Lett.,* 81 (2002) 3930

(176) J. Aarik, A. Aidla, K. Kukli and T. Uustare, *J. Cryst. Growth,* 144 (1994) 116

(177) K. Kukli, J. Aarik, A. Aidla, O. Kohan, T. Uustare and V. Sammelselg, *Thin Solid Films,* 260 (1995) 135

(178) J. Aarik, K. Kukli, A. Aidla and L. Pung, *Appl. Surf. Sci.,* 103 (1996) 331

(179) K. Kukli, M. Ritala, R. Matero and M. Leskelä, *J. Cryst. Growth,* 212 (2000) 459

(180) K. Kukli, J. Aarik, A. Aidla, K. Forsgren, J. Sundqvist, A. Hårsta, T. Uustare, H. Maendar and A. Kiisler, *Chem. Mater.,* 13 (2001) 122

(181) K. Kukli, M. Ritala and M. Leskelä, *J. Electrochem. Soc.,* 142 (1995) 1670

(182) K. Kukli, J. Aarik, A. Aidla, H. Siimon, M. Ritala and M. Leskelä, *Appl. Surf. Sci.,* 112 (1997) 236

(183) D. M. Hausmann, P. de Rouffignac, A. Smith, R. G. Gordon and D. Monsma, *Thin Solid Films,* 443 (2003) 1

(184) J. Sundqvist, H. Hoegberg and A. Hårsta, *Chem. Vap. Deposition,* 9 (2003) 245

(185) K. Kukli, M. Ritala and M. Leskelä, *Chem. Mater.,* 12 (2000) 1914

(186) J. Kwak, Y. Lee and B. Choi, *Appl. Surf. Sci.,* 230 (2004) 249

(187) Y. Lee, J. Kwak, B. Gang, H. Kim, B. Choi, B. Jeong, S. Park and K. Lee, *J. Electrochem. Soc.,* 151 (2004) C52

(188) M. Moisan and Z. Zakrzewski, *J. Phys. D: Appl. Phys.,* 24 (1991) 1025

(189) M. Moisan, J. Margot and Z. Zakrzewski in *High Density Plasma Sources: Design, Physics and Performance,* edited by Popov, Noyes, 1995, Park Ridge, New Jersey, U.S.A., p. 191

(190) T. M. Mayer, J. W. Rogers and T. A. Michalske, *Chem. Mater.,* 3 (1991) 641

(191) M. Ylilammi and T. Ranta-aho, *Thin Solid Films,* 232 (1993) 56

(192) R. A. Waldo, *Microbeam Anal.,* 23rd (1988) 310

(193) J. Jokinen, J. Keinonen, P. Tikkanen, A. Kuronen, T. Ahlgren and K. Nordlund, *Nucl. Instrum. Methods Phys. Res., Sect. B,* 119 (1996) 533

(194) S. J. Martin, J. P. Godschalx, M. E. Mills, E. O. Shaffer II and P. H. Townsend, *Adv. Mater.,* 12 (2000) 1769

(195) M. Ritala, P. Kalsi, D. Riihelä, K. Kukli, M. Leskelä and J. Jokinen, *Chem. Mater.,* 11 (1999) 1712

(196) M. Ritala, M. Leskelä, E. Rauhala and P. Haussalo, *J. Electrochem. Soc.,* 142 (1995) 2731

(197) S. M. Rossnagel and T. S. Kuan, *J. Vac. Sci. Technol. B,* 22 (2004) 240

(198) A. F. Mayadas and M. Shatzkes, *Phys. Rev. B,* 1 (1970) 1382

(199) M. Shatzkes, P. Chaudhari, A. A. Levi and A. F. Mayadas, *Phys. Rev. B,* 7 (1973) 5058

(200) S. Ram, *Infrared Phys. Technol.,* 42 (2001) 547

(201) Ritala Mikko, *Atomic Layer Epitaxy Growth of Titanium, Zirconium and Hafnium Dioxide Thin Films,* PhD Thesis, 1994, Helsinki

(202) Section 4: Properties of the Elements and Inorganic Compounds in CRC Handbook of Chemistry and Physics edited by David R. Lide, http://www.hbcpnetbase.com/